ChemComm

Accepted Manuscript

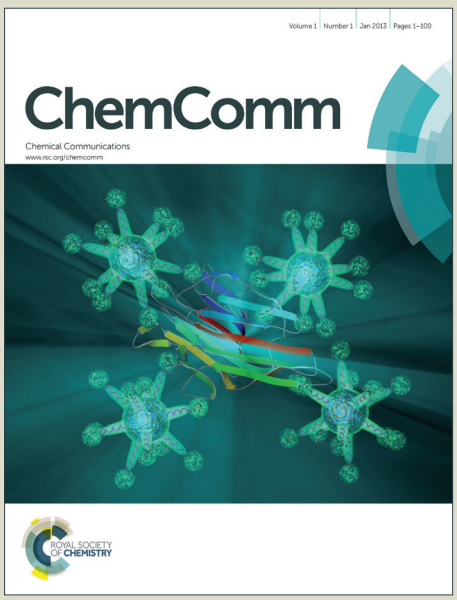

ROYAL SOCIETY OF CHEMISTRY

www.rsc.org/chemcomm

Mechanistic insights for the development of Li-O_2 battery materials: addressing Li_2O_2 conductivity limitations and electrolyte and cathode instabilities

Bryan D. McCloskey[a,b,*], Colin M. Burke[a,b], Jessica E. Nichols[a,b], Sara E. Renfrew[a,b]

[a]*Department of Chemical and Biomolecular Engineering, University of California, Berkeley, CA, 94720*

[b]*Environmental Energy Technologies Division, Lawrence Berkeley National Laboratory, Berkeley, CA, 94720*

*bmcclosk@berkeley.edu

Abstract

The Li-air battery has received significant attention over the past decade given its high theoretical specific energy compared to competing energy storage technologies. Yet, numerous scientific challenges remain unsolved in the pursuit of attaining a battery with modest Coulombic efficiency and high capacity. In this *Feature Article*, we provide our current perspective on challenges facing the development of nonaqueous Li-O_2 battery cathodes. We initially present a review on our understanding of electrochemical processes occurring at the nonaqueous Li-O_2 cathode. Electrolyte and cathode instabilities and Li_2O_2 conductivity limitations are then discussed and suggestions for future materials research development to alleviate these issues are provided.

TOC Figure

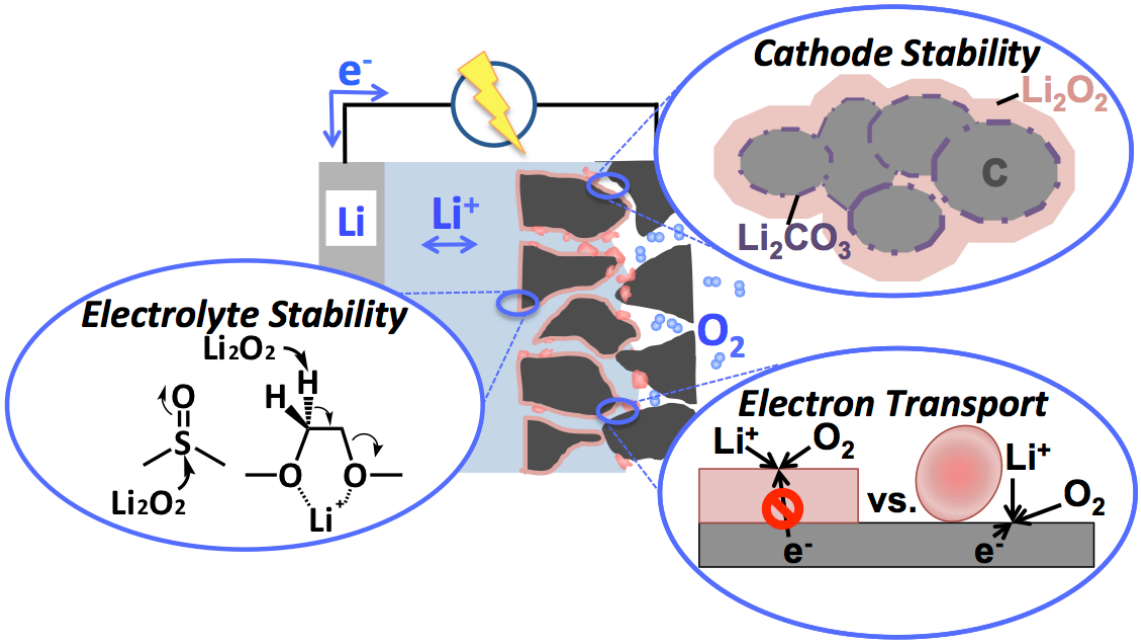

TOC text. This featured article provides a perspective on challenges facing Li-air battery cathode development, including Li_2O_2 conductivity limitations and instabilities of electrolyte and high surface area carbon.

1. Introduction

1.1 The need for new materials and chemistries for high energy, low cost batteries

A current focus in rechargeable battery research is identifying new materials or chemistries that could enable higher energy density and lower cost batteries than currently available Li-ion batteries.[1] These research directions are primarily driven by the understanding that, while still maintaining sufficient lifetime, safety, and power performance, a drastic reduction in battery cost and increase in battery energy density will be necessary to increase market penetration of electric vehicles.[2] Of course, improvements in rechargeable batteries would also be welcomed for other technologies, such as portable electronic devices and perhaps grid storage. Of the rechargeable batteries available, Li-ion batteries are used to power portable devices and electric vehicles because of their high energy density compared to other commercially available rechargeable batteries.[3, 4] Li-ion batteries were initially introduced to the portable electronics market in 1991 by Sony, and intense efforts to engineer the battery have since allowed incremental improvements in their performance. Yet, Li-ion electrode materials, which dictate attainable battery energy densities, used in these batteries have changed little in the past ~10 years; after enormous research efforts, the attainable limits in practical Li-ion battery energy density are therefore being approached.[5]

As a result, multiple research directions are now being pursued in hopes of advancing beyond the limits imposed by conventional Li-ion electrode materials. In the Li-ion field, new high-energy electrode materials, such as silicon anodes[6] and high voltage cathodes,[3, 4] are being developed. Other battery chemistries, including Li-O_2, Li-S, and Mg-ion, are also being explored given that their active cathode materials have high theoretical specific energies compared to Li-ion cathode materials (Table 1 provides a comparison of the electrochemical performance of Li_2S, Li_2O_2, and various Li-based metal oxides used as Li-ion battery cathode materials).[1, 7-16] Among the 'beyond Li-ion' battery cathode materials, Li_2O_2, the main discharge product of a nonaqueous Li-O_2 battery, has the highest theoretical specific energy and as a result, and in combination with the relatively low cost of the materials required to assemble the battery, has attracted significant research attention over the past decade.[17-20] It should be noted that although the values reported in Table 1 provide the impetus for Li-O_2 and Li-S research activity, more sophisticated treatments of realistic practical battery energy densities suggest only modest specific energy improvement, and no volumetric energy density improvement, may be achievable with fully developed Li-O_2 batteries over advanced Li-ion batteries (e.g., those using LMR-NMC and Li metal as the electrode materials).[21] Of course, this conclusion is contingent on the successful development of LMR-NMC and other high-energy Li-ion electrode materials, which are currently limited by fundamental challenges that result in voltage and capacity fade during extended cycling.[14, 16] Nevertheless, the objective of this featured article is to provide an honest assessment of our current understanding of the most pressing scientific challenges facing the nonaqueous Li-O_2 battery cathode. In particular, we will focus on challenges associated with instabilities of the electrolyte and cathode materials and Li_2O_2 electronic conductivity limitations. For brevity, we will omit in-depth discussion on the numerous engineering challenges (e.g., purifying air fed to the battery and protection of the Li metal anode) that also face the Li-O_2 battery, and note that reviews are available that provide a more complete account of these other challenges.[7, 19, 22] We will begin with a brief introduction on the nonaqueous Li-O_2 chemistry, followed by a discussion of our general understanding of stability

limitations that decrease battery rechargeability. We will conclude by describing Li_2O_2 formation mechanisms and their effect on attainable cell capacities, and will provide a perspective on interesting directions of future Li-air battery research throughout the article.

1.2 The Li-O_2 battery electrochemistry: Li_2O_2 formation and parasitic side reactions

The Li-O_2 battery chemistry. The active discharge electrochemistry in a Li-O_2 battery includes Li metal oxidation at the anode and oxygen reduction at the cathode. The exact reaction occurring at the cathode depends on the electrolyte employed. In aqueous electrolytes, where the Li metal anode is protected by a water impermeable, Li^+ conductive solid ion conductor, water also participates in the oxygen reduction reaction to form hydrated LiOH as the primary discharge product.[19] Water's involvement in the aqueous electrochemistry reduces the theoretical energy density of the aqueous Li-O_2 battery compared to the nonaqueous, aprotic Li-O_2 battery.[19, 23] Given this fact and the general complexities of protecting Li metal from aqueous solutions, less research has been devoted to the aqueous Li-air battery than the nonaqueous version, although interesting work to enable aqueous Li-air batteries is ongoing in numerous laboratories.[24-29] This article will focus on Li-O_2 batteries employing nonaqueous electrolytes with dissolved binary Li salts (a schematic of the nonaqueous Li-O_2 battery is shown in Figure 1).

A full galvanostatic (i.e., constant current) discharge-charge cycle for a typical nonaqueous Li-O_2 battery is shown in Figure 2, where panel a) presents the voltage profile, and panels b) and c) present quantitative measurements of the active electrochemical reactions occurring during discharge (panel b)) and charge (panel c)).[30] As was initially postulated by Abraham and Jiang in 1996,[31] the nonaqueous, aprotic Li-O_2 cathode discharge electrochemistry is predominantly, although not exclusively (for reasons explained below), the Li^+-induced $2e^-$ reduction of oxygen to form Li_2O_2 at the cathode, with Li metal oxidation occurring at the anode:

$$Li \leftrightarrow Li^+ + e^- \text{ (anode)} \quad (1)$$
$$2(Li^+ + e^-) + O_2 \leftrightarrow Li_2O_2 \text{ (cathode)} \quad (2)$$
$$2Li + O_2 \leftrightarrow Li_2O_2 \text{ (overall)} \quad (3)$$

Using various quantitative analytical techniques, the above reactions have been shown to occur in any reasonably stable nonaqueous, aprotic electrolyte in which water is not present,[32, 33] and even cells in which water is a trace impurity.[34, 35] For example, Figure 2b presents quantitative O_2 consumption, as measured using pressure decay in a known cell headspace volume, and concomitant Li_2O_2 formation, measured using an established peroxide titration, during a galvanostatic discharge of a cell employing an ether-based electrolyte and a carbon-based cathode. In this cell, a nearly 2 e^-/O_2 process is observed, consistent with reaction 2 above. A similar ~2 e^-/O_2 process on discharge is observed in many other nonaqueous electrolytes, as is presented in Table 2.[32]

Given this 2 e^-/O_2 process, we would expect, and indeed numerous reports have confirmed, Li_2O_2 formation consistent with equation 2. However, the efficiency of O_2 conversion to Li_2O_2 is less than ideal for all nonaqueous electrolytes/electrode configurations studied to date; the discrepancy between O_2 consumption and Li_2O_2 formation is observed in Figure 2b, where 2.41 e^- are necessary to form each Li_2O_2 molecule, whereas 2.02 e^- are consumed for each O_2 molecule (2.00 e^- per Li_2O_2

and O_2 is expected from equation 2). Using numerous spectroscopic and quantitative analytical techniques, this discrepancy is attributed to irreversible reactions between Li_2O_2 and the electrolyte and is generally observed to varying degrees for different electrolyte/cathode configurations (as is shown in Table 3).[30, 33, 36, 37] Of note, the 4 e^- oxygen reduction product, lithium oxide (Li_2O), and the $1e^-/O_2$ product, lithium superoxide (LiO_2), have not been spectroscopically observed as ultimate discharge products in nonaqueous Li-O_2 batteries, although LiO_2 has been observed as an intermediate to Li_2O_2 formation.[38] Recent reports have indicated that a 'LiO_2-like' species is present in the ultimate discharge product in high surface area carbon electrodes,[39, 40] but the raman peaks ascribed to these LiO_2 species are in fact related to decomposition of the electrode binder (poly(vinylidene fluoride)), which occurs during discharge of a cell in which minor water impurities are present in the electrolyte.[7]

On charge, the reverse reactions in equations 1-3 are expected, with Li_2O_2 oxidation to O_2 occurring at the cathode and Li^+ reduction to Li metal occurring at the anode. Figure 2c) compares Li_2O_2 oxidation and O_2 evolution during a typical galvanostatic charge. Although all Li_2O_2 formed during discharge was found to oxidize, less O_2 is evolved than Li_2O_2 oxidized, indicating that parasitic processes are occurring during charge. The parasitic reactions occurring during battery operation will be discussed more completely in section 2, but it is important to understand that in appropriately selected nonaqueous electrolyte/electrode configurations, the cathode electrochemistry is dominated by O_2 reduction/evolution and Li_2O_2 formation/oxidation during discharge/charge, respectively.

The prominent features of a galvanostatic Li-O_2 battery discharge-charge cycle. A full galvanostatic discharge-charge cycle potential profile is shown in Figure 2a and exhibits the following features usually observed in most Li-O_2 battery studies:

1. The discharge profile exhibits a broad voltage plateau below the equilibrium, open circuit potential of the cell (U~2.85 V vs. Li/Li^+). The exact voltage of this plateau is a function of many different cell parameters, including the electrolyte employed, the cathode surface area, and the oxygen partial pressure. The plateau voltage is also dependent on the current rate for a given cell composition, with higher current rates leading to lower voltages.
2. At some capacity (in mAh) well below the theoretical capacity of the Li-O_2 chemistry, the voltage of the cell during discharge precipitously drops, a process that has been termed 'sudden death' in previous publications.[41, 42] The capacity at which sudden death occurs is also a function of the cell parameters listed in '1.'
3. The reverse reactions of equations 1-3 ideally occur during charge at potentials higher than the cell open circuit potential. Initially, the charge potential generally proceeds at a low potential (<3.5V), close to the cell's open circuit potential. This initial potential can be as low as 2.9 V, if charging a cell that was discharged to less than its sudden death capacity (e.g., see Figure 4 and 5).[43] As the charging process proceeds, the cell potential continuously increases to an ultimate voltage of >4.5 V. As will be described in Section 2.3, many report that the high ultimate charging potential is a result of sluggish Li_2O_2 oxidation kinetics and suggest electrocatalytic solutions to this problem. The high potential is actually a result of ever decreasing surface area for oxygen evolution and a mixed potential caused by parasitic side reactions.[44]

It is worth considering these features compared to what is expected during an ideal discharge-charge process. Ideally, the discharge potential would be nearly identical to the open circuit potential and would only slightly decrease as the current rate increased, implying fast transport and reaction kinetics. The discharge would continue until all Li metal contained in the anode were oxidized, assuming oxygen was abundantly available. For comparison, the cell discharged in Figure 2 contained Li metal equivalent to roughly 50 mAh. For the duration of charge, the cell potential would remain only slightly above the open circuit potential of the cell and only slightly increase as current rate increased, once again implying fast transport and reaction kinetics. The voltage profile would not change over the cycle lifetime of the battery (e.g., cycle 1 and 1000 would exhibit the same voltage profile and electrochemistry). This discharge-charge profile behavior is ideal for three reasons: 1) the small voltage gap between the discharge and charge processes results in nearly the same amount of energy delivered during discharge as is required to charge the cell (i.e., energy efficiency close to 100%), 2) all Li is consumed, resulting in the highest possible electrochemical capacity being extracted from the system, 3) no capacity or voltage fade at high depth of discharge implies that no parasitic reactions are occurring in the cell.

Evident questions are then: why is the observed discharge-charge profile markedly different than the ideal profile, and what is limiting the cell from achieving this ideal, or at least close-to-ideal, behavior? We hope to convey that the observed profile is dictated by Li_2O_2 formation at the cathode and its resultant effect on the electrochemical and chemical processes occurring in the cell. Specifically, Li_2O_2 is a strong oxidizer and, as discussed earlier, presents stability limitations with the organic electrolytes and cathodes with which it comes into contact. Additionally, Li_2O_2 is both a wide bandgap insulator and generally insoluble in nonaqueous electrolytes. It therefore deposits on and electronically passivates the cathode surface, limiting the overall capacity. The following sections will discuss these two challenges and how they relate to the features shown in Figure 2.

2. Stability of nonaqueous electrolytes and cathode materials

2.1 The definition and measurement of rechargeability in Li-O_2 batteries

In combination with the ideal voltage profile discussed in the previous section, the following statement captures our chemical definition for ideal Li-O_2 battery rechargeability: during a galvanostatic discharge-charge cycle, where the discharge and charge capacity are equal, all O_2 reduced during discharge (ORR) is evolved during charge (OER), and this O_2 reduction/evolution remains constant during extended cycling. In other words, a perfectly rechargeable system would be one in which OER/ORR=1, and the total amount of oxygen reduced would be equal for each galvanostatic cycle during the lifetime of the cell. This definition also implies that the following points are true:

1. Li metal plating stripping is 100% efficient (i.e., all Li oxidized during discharge is re-plated during charge), such that Li is not irreversibly consumed by parasitic reactions during cycling. If Li is lost irreversibly during cycling, the capacity of the cell would decrease with cycle number once all excess Li metal is consumed.
2. Electrons consumed or liberated during the electrochemical processes at the battery cathode only contribute to ORR and OER and not to other parasitic reactions, such as CO_2 and H_2 evolution, or carbonate/carboxylate formation.

3. From a rechargeability perspective, Li_2O_2 formation during discharge is not necessarily a requirement for a rechargeable Li-O_2 battery. It is, however, the only possible Li-O_2 battery discharge product that we have identified that evolves O_2 at oxidative potentials on carbon electrodes at room temperature (LiOH, Li_2CO_3, and Li_2O have been found to not evolve O_2 during oxidation in nonaqueous electrolytes).[45] Therefore, only Li_2O_2 should form during discharge and only O_2 should be evolved during oxidation (charge) of Li_2O_2. Nevertheless, other cell configurations (perhaps those employing exotic cathodes and electrolytes) in which ORR products other than Li_2O_2 are formed (e.g., Li_2O) and evolve O_2 during oxidation could in theory be envisioned.

As discussed earlier, and shown in Figure 2 and Tables 2 and 3, significant parasitic decomposition processes, both electrochemical and chemical in nature, are typical for Li-O_2 batteries, unlike Li-ion batteries, in which the reversible insertion of Li^+ into graphite and high voltage hosts are accompanied by significantly fewer side reactions. Therefore, capacity or voltage fade from cycle-to-cycle, as is typically used in the Li-ion field, is not an appropriate metric for stability, particularly when a large excess of Li metal is used as the anode (as is nearly always the case in published studies of Li-O_2 electrochemistry), which can accommodate modest component decomposition by replenishing lithium lost to parasitic reactions. Furthermore, parasitic reactions occur in Li-O_2 cells at the same potentials as Li_2O_2 formation and oxidation, and with poorly selected electrocatalysts, these parasitic reactions can actually occur at potentials very close to the Li_2O_2 oxidation equilibrium potential, leading to misguided conclusions about the efficacy of Li_2O_2 oxidation electrocatalysis.[43] It is therefore absolutely critical to combine quantitative measures of chemical reversibility with electrochemical characterization in order to definitively prove that an improvement in battery rechargeability or a reduction in Li_2O_2 formation/oxidation overpotential is observed.

Many reports on Li-O_2 battery rechargeability have realized the importance of combining product formation characterization with battery cycling. Typically, these reports use various spectroscopic techniques to show that an unspecified amount of Li_2O_2 forms during discharge and oxidizes during charge over many cycles. Yet, many spectroscopic techniques have limited sensitivity and therefore cannot detect minor parasitic product formation. An example is X-ray diffraction on cathodes discharged in carbonate electrolytes, where no products are observed using diffraction even though substantial amounts of solid alkyl carbonates are known to form.[45] Even if Li_2O_2 is exclusively observed using a certain spectroscopic technique, care must be taken when assessing rechargeability using this result, as the amount of Li_2O_2 formed is unknown and may not necessarily be consistent with the amount of charge passed during a discharge. Given the requirement of OER/ORR=1 for a truly rechargeable Li-O_2 battery, measurements of gas consumption and evolution are essential. Pressure decay/rise measurements in a known cell headspace volume (as shown in Figure 2) and differential electrochemical mass spectrometry (DEMS) can both be used to fully quantify gas consumption and evolution during Li-O_2 battery operation.[45-47] Any claims of battery rechargeability are inadequate without similar measurements.

2.2 Nonaqueous Li-O_2 electrolyte stability

Perhaps the most important current direction of Li-O_2 battery research is the search to identify an appropriate electrolyte/electrode combination that results in long-term battery

rechargeability. Initial efforts in this area were spurred by the unfortunate discovery that liquid carbonate electrolytes, those prevalent in Li-ion batteries, were entirely unstable towards the active Li-O_2 battery electrochemistry, producing primarily solid lithium carbonate species on the surface of the cathode during discharge and evolving little O_2, but significant CO_2, during charge.[45, 48-51] Since, many different electrolyte solvents and salts have been characterized for stability in the presence of reduced oxygen species.[32, 52-55] We are currently unaware of an organic liquid electrolyte-based Li-O_2 battery that conforms to the chemical definition of rechargeability given in section 2.1.

A few studies highlight the difficulties of identifying such stable electrolytes. Bryantsev et al. have combined ab-initio calculations of electrolyte stability towards superoxide radicals with chemical and electrochemical measurements of oxygen reduction/evolution in Li-bearing electrolytes using a variety of organic solvent classes, including amides, nitriles, oxygenated phosphorus compounds, fluorinated ethers, sulfonates, esters, lactones, and sulfones.[56-58] From these studies, they identified amides, particularly dimethylacetamide with $LiNO_3$ employed as the salt, to exhibit the highest stability amongst all explored electrolytes.[59, 60] They used this electrolyte to produce a battery that could be cycled 80 times (with O_2 being confirmed as the primary gas evolved during charge on the 2nd, 40th, and 80th cycle) when a limited depth-of-discharge was utilized, as shown in Figure 3. Nevertheless, parasitic losses restricted the long-term cyclability (>100 cycles) of this optimized battery composition, and full depth-of-discharge yielded a battery with dramatic capacity fade over the first 5 cycles.

McCloskey et al. measured the OER/ORR values for the first galvanostatic discharge of many different electrolytes with varying salts and solvents, including ethers, amides, nitriles, and ionic liquids, while employing carbon electrodes, as shown in Table 2.[32] No electrolyte was found to yield an OER/ORR value greater than 0.9 in the first galvanostatic cycle, which is poor considering Li-ion battery Coulombic efficiencies routinely surpass 0.999. McCloskey et al. likened the issue of organic electrolyte stability as being stuck between a 'rock and a hard place,' in reference to the anti-correlated electrolyte requirements of being impervious to Li_2O_2/LiO_2-induced nucleophilic attack (requiring low electron affinity) during discharge and having high electrochemical oxidative stability in the presence of Li_2O_2 (requiring high ionization potential) during charge. In fact, as is observed in Figure 2, decomposition of ether-based electrolytes, which McCloskey et al. found to be among the most stable solvents for Li-O_2 batteries, occurs on both discharge and charge, implying that both nucleophilic attack and high-voltage oxidation are prevalent mechanisms for parasitic reactions even in electrolytes which exhibit reasonably high stability.[30]

In a series of articles, Bruce and co-workers have explored numerous classes of electrolytes, including carbonates,[49] ethers,[61] amides,[62] sulfones,[63] and dimethyl sulfoxide (DMSO).[64] Although these electrolytes exhibited varying extents of cyclability, none were found to be stable using a carbon-based cathode. However, Peng et al. reported that, when using a nanoporous gold cathode, DMSO/$LiClO_4$-based electrolytes promoted the desired 2.0 e^-/O_2 electrochemistry on both discharge and charge for 100 cycles.[64] Many subsequent reports have indicated that DMSO is chemically unstable in the presence of Li_2O_2, and attempts to reproduce the cyclability of cells employing DMSO-based electrolytes have proven difficult as a result.[30, 65-68] Nevertheless, Peng et al.'s report highlights the fact that electrolyte stability is clearly affected by the composition of the

cathode employed. This electrode/electrolyte interaction is worth discussing more completely in the context of heterogeneous electrocatalysis and cathode stability (sections 2.3 and 2.4).

However, no organic electrolyte has been convincingly shown to produce the reversible Li-O_2 electrochemistry. Researchers have pointed to numerous possible nonaqueous electrolyte decomposition mechanisms, depending on the identity of the organic solvent, including O_2^--induced nucleophilic substitution,[58] O_2^- and Li_2O_2-induced hydrogen and/or proton abstraction,[56, 69-71] Li_2O_2-induced Dakin-type oxidation,[72] simple electrochemical oxidation at high voltages,[45] and autoxidation.[57]

The search for a stable electrolyte. With organic solvents posing significant stability challenges, many interesting directions of research are aimed at identifying inorganic electrolytes that provide extended Li-O_2 battery rechargeability. Solid state ion conductors, such as garnet phase $Li_7La_3Zr_2O_{12}$ (LLZO) and $Li_xAl_{2-y}Ti_y(PO_4)_3$ (LATP), as electrolytes may serve a dual purpose of improving the stability of both the cathode and anode electrochemistry.[25, 28, 73-76] Large research efforts are currently underway to develop these electrolytes for Li metal based batteries because their mechanical rigidity may suppress Li dendrite formation.[77] In Li-air batteries, they would serve another beneficial purpose: they are impermeable to gases and would therefore eliminate parasitic reactions between Li and O_2/N_2. Certain solid ion conductors, such as $Li_{10}GeP_2S_{12}$ (LGPS),[78] have also been reported to be very robust at high potentials, which could potentially allow improvements in cathode stability. However, implementation of solid state conductors would present many engineering challenges, including the design of a Li_2O_2-accommodating, high surface area, low interfacial resistance porous cathode, processability at thicknesses (10-20 microns) required to ensure competitive energy densities, and stability towards Li metal, where a buffer layer may need to be engineered to eliminate electrolyte reduction and improve interfacial stability with certain solid state formulations (such as LATP and LGPS).[79, 80]

Molten inorganic salts, such as the $LiNO_3/KNO_3$ eutectic (melting point ~127 ^oC), are an interesting route of electrolyte research, as is being explored by Liox.[81] Here, the organic solvent that is susceptible to Li_2O_2-induced degradation is completely removed from the electrolyte composition. Operating at elevated temperatures may also serve to enhance Li_2O_2 conductivity, thereby improving cell capacity (see section 3), although obvious engineering challenges of high temperature battery operation also exist. More research on Li-O_2 batteries employing these electrolytes is necessary to judge overall electrochemical performance.

Potential electrolyte compositions containing organic solvents, ionic liquids and polymers may warrant further study, although concerns remain about the stability of these materials given their organic nature. In particular, numerous ionic liquids still remain to be explored for Li-air batteries, and already many have been reported to have very high oxidation potentials in Li-ion batteries.[82-84] Polymer electrolytes may also provide a route to stabilize decomposition reactions occurring at the cathode/electrolyte interface.[85] Regardless, the design of organic electrolytes must conform to a stringent set of properties to maintain reasonable stability while still allowing modest ionic conductivity. Khetan et al. provided theoretical insight into the proper design of electrolyte solvents, indicating that a solvent's acid dissociation constant, a measure of its susceptibility to deprotonation/ H-abstraction, and highest occupied molecular orbital (HOMO) level, which was used as a measure of the solvent's oxidative stability, could both be used as useful, easily accessible properties to screen the potential stability of organic electrolytes.[86, 87] Here, high pKa (low

deprotonation susceptibility) and low HOMO energies (oxidatively stable) are desired, and unfortunately typically anti-correlated, properties for stable solvents. The search for stable organic electrolytes should focus on identifying outliers to this anti-correlated trend.

2.3 Heterogeneous electrocatalysts: sluggish Li_2O_2 oxidation kinetics or mixed oxidation potential?

Given the large overpotential during charge, significant amounts of research currently focus on employing heterogeneous electrocatalysts in an attempt to improve the ostensible sluggish kinetics of O_2 evolution from Li_2O_2.[88, 89] However, compelling evidence, both experimental and theoretical,[44] indicates that the generally observed ever-increasing charge potential (Figure 2a, 4, and 5) is actually related to the deposition and accumulation of decomposition products at the Li_2O_2/electrolyte interface and not due to the inherent sluggish kinetics of O_2 evolution from Li_2O_2, which in fact appear to be remarkably fast.[90, 91] Three key observations, among others discussed in Viswanathan et al.,[90] lead us to this conclusion: 1) O_2 evolution from Li_2O_2 actually occurs most efficiently (i.e., closest to 2 e^-/O_2) at the early stages of charge, where the cell voltage is its lowest (Figure 4a and b); 2) O_2 evolution decreases as charge proceeds, indicating parasitic reactions increasingly contribute to the electrochemistry; 3) lithium carbonates were observed to accumulate at the cathode as charge proceeds.[30, 92] The interfacial carbonate formation in the electrode leads to an ever-decreasing amount of Li_2O_2 present at the oxygen-evolving surface. As a result, the current per unit of active area during OER dramatically increases, which necessarily drives the OER potential to increasingly higher values as carbonate surface coverage increases.[44] Once the potential is sufficiently high (>4V), CO_2 evolution from carbonates will occur concomitantly with O_2 evolution from Li_2O_2.[93]

Electrocatalysts can also promote parasitic side reactions occurring in the cell by enhancing oxygen reactivity with the electrolyte during discharge, or lowering oxidation potentials for CO_2 evolution through many different electrolyte decomposition pathways. As shown in Figure 4, McCloskey et al. observed that incorporation of certain electrocatalysts, such as Au, Pt, and MnO_2, leads to higher decomposition rates and less O_2 evolution than pure carbon cathodes for cells employing ether-based electrolytes.[43] Pt was a particularly active electrocatalyst for promoting solvent decomposition, leading to significantly less O_2 evolution, and therefore a poor OER/ORR value, and a much lower potential for CO_2 evolution than the other catalysts. Nasybulin et al. observed that Li-O_2 cells with cathodes employing carbon nanotubes decorated with Ru nanoparticles could be cycled 50 times, but with ever increasing CO_2 evolution during each subsequent charge (Table 4).[94] A very important judgement is that electrocatalysts that are even modestly active towards the O=O bond splitting necessary to enhance the 4e^- aqueous oxygen reduction reaction are likely poor candidates for electrode materials in nonaqueous Li-O_2 batteries, where a 2 e^- oxygen reduction process is observed. These catalysts, typically employed in fuel cells, include Pd, Pt, Ru, and MnO_2, and related alloys.

Furthermore, as will be discussed in section 3, Li_2O_2 is insoluble in organic electrolytes and therefore coats the cathode surface as it is formed, blocking catalytic sites from being accessed during charge. Although a fraction of the deposited Li_2O_2 may still be in contact with catalytic sites, Li_2O_2 not in contact with catalytic sites is precluded from transporting back to catalytic sites (if they were accessible) during charge by its insolubility. These issues highlight the fact that instead of

focusing on improving nonaqueous OER electrocatalysis, a more pressing research direction to reduce OER overpotentials is to eliminate electrolyte and cathode (section 2.4) degradation in the presence of Li_2O_2, which is a significant challenge for organic-based components.

2.4 Positive electrode stability

Carbon electrodes. Most Li-O_2 electrodes are comprised of at least a small amount of high surface area particulate carbon, perhaps with another high surface area material, bound to a current collector using a polymer, due to carbon's desirable Li-O_2 battery electrode properties, including high conductivity, high electrochemically-available surface area, and affordability. Unfortunately, stability limitations have been identified for both the carbon and polymer in a Li-O_2 battery cathode. McCloskey et al. and Thotiyl et al. used isotopically labeled particulate carbon to decouple decomposition products forming from the cathode and the electrolyte.[44, 92] Figure 5a presents a galvanostatic discharge-charge using a 99% ^{13}C-labeled cathode and a ^{12}C-DME/LiTFSI electrolyte. CO_2 evolution on charge (Figure 5b) is clearly observed from both the cathode and the electrolyte. Using X-ray photoelectron spectroscopy, Gallant et al. and Itkis et al. identified that a thin Li_2CO_3 layer formed on a carbon cathode surface during cell cycling.[95, 96] The Li_2CO_3 was found to form at high potentials during charge in the presence of Li_2O_2 by Thotiyl et al.,[92] whereas McCloskey et al. found that carbon oxidized from the very initial stages of the charging process, even at low oxidative potentials.[44] However, carbon appeared to be reasonably stable during discharge, as shown using NMR by Xu et al. and a carbonate titration by Thotiyl et al.[33, 92] This is somewhat surprising, as the reaction between lithium peroxide, oxygen, and carbon to form Li_2CO_3 is very thermodynamically favorable (ΔG_{rxn}=-542 kJ/mol), although appears to be kinetically hindered at open circuit or reductive potentials.[44] Although the precise mechanism of carbon oxidation is unknown, a combination of ^{13}C and ^{18}O labeling of the carbon and discharge gas atmosphere, respectively, indicated that a significant quantity of the oxygen (~33%, Figure 5c) in the Li_2CO_3 formed from carbon decomposition originated from the electrolyte, indicating that reactive species are formed at the Li_2O_2/electrolyte interface and then diffuse to, and react with, the carbon surface.[44]

Polymer binders. Stability of polymer binders is also a concern, although certain polymers have been identified to provide at least reasonable resistance to Li_2O_2-induced decomposition. Initial studies employed primarily poly(vinylidene fluoride) as an electrode binder given its ubiquity in the same capacity in Li-ion batteries. However, Black et al. identified its chemical instability towards Li_2O_2 and other reduced oxygen species.[97] The chemical stability of many other polymers in the presence of Li_2O_2 has been explored by Nasybulin et al. and Amanchukwu et al., with polyethylene and perfluorinated polymers being identified as reasonably stable.[98, 99] McCloskey et al. also characterized Nafion and polytetrafluoroethylene-bound electrodes and found Li_2O_2 yield during discharge using these electrodes to be reasonably similar to binderless electrodes (Table 3), implying that electrochemical irreversibilities are predominantly related to the electrolyte or carbon instabilities and not binder instabilities.[30]

Carbon and binder-free electrodes. Realizing the stability limitations of carbon and polymer binders, many reports now exist for carbon-free and/or binder-free Li-O_2 battery cathodes. As discussed previously, Peng et al. used a nanoporous pure gold cathode and reported improved rechargeability over carbon-based cathodes when employing DMSO and ether-based electrolytes.[64]

In further attempts to identify a more cost-effective alternative to a pure gold cathode, Thotiyl et al. identified TiC as a reasonable replacement for carbon, with further studies by Adams et al. promoting TiC's viability as a cathode material.[100, 101] Freestanding cobalt oxide (Co_3O_4) and $NiCo_2O_4$ electrodes have also been synthesized and reported to improve rechargeability.[102-104] Coating carbon with a thin layer of a potentially inert material has also been used as a cathode protection strategy, with both Al_2O_3 and FeO_x being deposited on carbon cathodes using atomic layer deposition.[105, 106] Of note, the chemical stability of the electrolyte is still a critical challenge when characterizing the stability of the electrode, and can overwhelmingly contribute to the parasitic reactions observed in the cell. For example, when characterizing TiC electrodes, Luntz and McCloskey still observed OER/ORR values similar to those observed for carbon cathodes for both DMSO and ether-based electrolytes, implying that cell rechargeability is primarily governed by the stability of the electrolyte.[7] Nevertheless, the search for a cost-effective, stable, and electrocatalytically inactive alternative to porous carbon is an important direction of research facing Li-air battery development.

3. Li_2O_2 insulation and capacity limitations in Li-O_2 batteries

Li_2O_2 is a known wide band gap insulator and is insoluble in aprotic organic electrolytes, so it is no surprise that Li_2O_2 electronically passivates the cathode as it is formed.[7, 42, 107, 108] This electronic passivation eventually results in the 'sudden death' observed in Figure 2 at a fraction of the theoretically attainable capacity. However, recent studies have shown that certain Li_2O_2 deposition mechanisms can circumvent this electronic passivation, which ultimately improves achievable battery capacity.[34, 109] Although a few Li_2O_2 deposition mechanisms have now been postulated, they fall into one of two broad categories, which we will refer to as surface-based or solution-based mechanisms. We will discuss each of these categories, including their effect on cell capacity and our understanding of the cell properties that affect the predominance of each during discharge.

3.1 The mechanisms of Li_2O_2 deposition

In all nonaqueous Li^+-bearing electrolytes that exhibit modest stability, Li_2O_2 has been identified as the primary discharge product. The mechanism for Li_2O_2 formation occurs in multiple steps and is known to be influenced by the electron donating and accepting properties of the electrolyte. Generally, electrolytes with low Gutmann donor or acceptor numbers (measures of Lewis basicity and acidity, respectively) promote a 'surface' mechanism, whereas electrolytes with high donor (DN) or acceptor numbers (AN) promote a 'solution' mechanism.[34, 109-111]

Regardless of the electrolyte composition, the first step in Li_2O_2 formation proceeds by oxygen diffusing and binding to active sites on the cathode surface, then reacting with Li^+ in a concerted electrochemical reaction to form surface-bound LiO_2:

$Li^+ + e^- + O_2^* <--> LiO_2^*$ (* denotes a surface bound species) (4)

$O_2 + e^- = O_2^-$ has also been postulated as a potential first ORR step in Li^+-bearing nonaqueous electrolytes, with a subsequent, temporally-separated solution phase chemical reaction of O_2^- with Li^+ to form LiO_2. However, reaction 4 is rationalized to be the first step in Li_2O_2 formation because

the onset potential of oxygen reduction in Li^+ electrolytes is shifted positively when compared to oxygen reduction in electrolytes that employ identical solvents, but with cations (e.g., tetraalkyl ammonium) that promote the 1 e^-/O_2 formation of soluble O_2^- as the ultimate ORR product (Figure 6). This positive potential shift implies that the thermodynamic stability of LiO_2* is greater than solvated O_2^-, inferring that the concerted electrochemical reaction of Li^+ with O_2 to form LiO_2* has to be the initial step in Li_2O_2 formation in all Li^+-bearing nonaqueous electrolytes. Formation of the soluble O_2^- as a first step would imply that the solution mechanism should dominantly occur in any electrolyte, including those with low Lewis acidity and basicity, which does not seem to be the case even for electrolytes with moderate donor/acceptor properties.[34, 38, 112, 113]

However, O_2^- has in fact been observed as an intermediate to Li_2O_2 formation in high Lewis basic (high DN) Li^+ electrolytes using surface enhanced raman spectroscopy (SERS), electron paramagnetic resonance, and ring-disk voltammetry.[109, 112, 114] This observation is coupled with a significant decrease in the magnitude of the ORR potential shift between Li^+ and ammonium-bearing electrolytes as the Lewis basicity of the electrolyte solvent increased. For example, the cathodic onset potential differences in the DMSO electrolytes (~70mV between the 100 mM NBu_4^+ and 100 mM Li^+ electrolytes) in Figure 6b) are much smaller than the onset potential difference in the DME electrolytes in Figure 6a) (~250 mV).[109, 113] These results suggest that Li^+ is more effectively stabilized in high Lewis basic electrolytes (such as the DMSO electrolytes), such that LiO_2* dissolves in the electrolyte via:

$$LiO_2^* \text{ <--> } Li^+(sol) + O_2^-(sol) \quad (5)$$

LiO_2* dissolution is the obvious requirement for the solution mechanism for Li_2O_2 formation. LiO_2* dissolution can occur either through enhanced stabilization of solution soluble Li^+ or O_2^-, which is known to be accomplished by increasing either the DN or AN, respectively, of the electrolyte. Laoire et al. originally observed that the battery discharge mechanism was affected by the electron donating power of the electrolyte,[110, 111] and Johnson et al. later confirmed a positive correlation between electrolyte donor number and solution mechanism enhancement.[109] Aetukuri et al. found that the inclusion of minor water impurities also promoted the solution-based mechanism in electrolytes that otherwise did not have a sufficient Lewis basicity or acidity to support the solution process.[34] They hypothesized that water's strong Lewis acidity (AN= 54.8) stabilized O_2^-, leading to an enhancement in the solution mechanism.

LiO_2 dissolution appears to be nearly instantaneous in high DN electrolytes, as only O_2^- and no LiO_2 is observed on a roughened gold electrode using SERS.[109] If appropriately stabilized, soluble O_2^- will diffuse away from the site at which it was initially formed, allowing the active cathode site for ORR to remain accessible to Li^+, O_2, and e^-, the implications of which will be discussed in more detail below. It is known that even when the solution mechanism is prevalent during discharge, the ultimate discharge product is Li_2O_2, such that O_2^- (sol) likely diffuses to the surface of nucleated Li_2O_2 particles on the cathode surface and undergoes disproportionation to grow solid Li_2O_2 during the final step of the solution mechanism, *i.e.*:

$$2Li^+ + 2O_2^- (sol) \rightarrow Li_2O_2(s) + O_2 (g) \quad (6)$$

Reactions 4, 5, and 6 combine to form the elementary reactions believed to be prevalent in the solution mechanism.[34, 109] In contrast, electrolytes with low Gutmann donor or acceptor numbers do not promote LiO_2* solubility. Therefore, one of two processes (aside from parasitic side reactions with the electrolyte, as discussed previously) necessarily occurs after LiO_2 forms given that it is unstable at room temperature:[115] another Li^+-induced charge transfer to form Li_2O_2*, or disproportionation of LiO_2* to Li_2O_2* and O_2:

$Li^+ + e^- + LiO_2^* \rightarrow Li_2O_2^*$ (7a)
or
$2LiO_2^* \rightarrow Li_2O_2^* + O_2$ (7b)

Reactions (4), (7a), and (7b) comprise the surface mechanism for Li_2O_2 formation.

3.2 Promoting the solution mechanism for Li_2O_2 deposition improves cell capacity

The importance of the mechanism on battery performance is clear when comparing the capacity of cells employing different electrolytes. Figure 7a presents the discharge profiles of cells employing electrolytes comprising lithium perchlorate dissolved in acetonitrile (DN= 14 kcal/mol), dimethoxyethane (DN= 20 kcal/mol), DMSO (DN=30 kcal/mol), or 1-methylimidazole (DN= 47 kcal/mol).[109] As the donor number of the electrolyte increases, the solution mechanism is increasingly promoted and the surface mechanism increasingly demoted, thereby increasing cell capacity. A similar effect was observed in cells with trace water impurities, with an increasing water content leading to increasing cell capacities (Figure 7b).[34, 35, 116]

SEM images of discharged cathodes reveal the cause of the capacity differences in cells with dominant surface or solution mechanisms; Figure 8 presents images of cathodes discharged in 1M LiTFSI in DME electrolytes with varying water contents.[34] It should be noted that Li_2O_2 was confirmed to be the primary discharge product in water contaminated cells, with Li_2O_2 yields similar to nominally anhydrous cells.[34, 35] LiO_2* surface diffusion lengths are likely to be very small considering LiO_2's short lifetime, such that the surface mechanism reactions lead to Li_2O_2 deposition at the sites of initial LiO_2 formation. Given that Li_2O_2 eventually electronically insulates the sites at which it is formed, the surface mechanism results in a conformal coating of Li_2O_2 on the cathode surface, such that pristine and discharged cathode morphologies appear similar (Figure 8a). The electronic resistance imparted by the growing conformal Li_2O_2 layer leads to a large, sudden voltage drop at some capacity significantly below the theoretical capacity for the battery. This effect is observed in Figure 2a, where the voltage at the end of the discharge cycle falls precipitously. Using electrochemical impedance spectroscopy (Figure 9), Hojberg et al. ascribed this 'sudden death' of cells employing 1M LiTFSI in DME, an electrolyte that fully promotes the surface mechanism, to a very large increase in the charge transfer resistance during oxygen reduction at the cathode (R_3 in Figure 9 is related to charge transfer during the oxygen reduction process).[117] Viswanathan et al. hypothesized that hole tunneling is primarily responsible for charge transport through Li_2O_2 films during discharge, and a critical film thickness of roughly 5 nm is sufficient to arrest hole tunneling, leading to cell sudden death.[41] In support of this finding, Meini et al. observed a nearly linear correlation between cathode surface area and ultimate discharge capacity in a surface mechanism-promoting ether-based electrolyte, with the capacity being consistent with a roughly 2 monolayer

(~1 nm) thick Li_2O_2 conformal coating.[118]

In contrast, cells in which the solution mechanism is dominant, large (100-1000 nm) Li_2O_2 toroids are clearly observed,[119, 120] indicating that Li_2O_2 growth at least partially circumvents the passivation observed when the surface mechanism dominates. Similar trends in Li_2O_2 deposition morphology were observed with increasing electrolyte DN.[109] However, the same 'sudden death' is observed in these cells, implying that Li_2O_2 electronic passivation also limits cell capacity when the solution mechanism is dominant, albeit after significantly more Li_2O_2 has been formed. Further electrochemical impedance analysis is necessary to conclusively confirm the origin of the 'sudden death' in cells where the solution mechanism is dominant.

The search for a high capacity electrolyte. Electrolyte engineering to promote the solution Li_2O_2 formation mechanism during discharge clearly provides a potential route to circumventing Li_2O_2 conductivity limitations. Unfortunately, there is a tradeoff between an electrolyte's ability to promote the solution mechanism and its stability in the presence of the Li-O_2 electrochemistry, as was recently theoretically described by Khetan et al.[70] For example, DMSO is observed to effectively promote the solution mechanism, thereby leading to high cell capacities. However, as discussed previously, DMSO is also a poorly stable electrolyte solvent. In fact, the increase, or decrease, in capacity of cells employing certain electrolytes likely can be affected by substantial parasitic side product formation, particularly if the side products formed are soluble in the electrolyte. An interesting direction of research includes the identification of electrolyte salts that enhance the solution process. Specifically, the Li^+ counteranion has also been found to influence the predominance of either the surface or solution mechanism, given that the anion also plays a role in stabilization of Li^+ in solution.[121, 122] The anion could in theory be designed to be more stable to the Li-O_2 electrochemistry than the electrolyte solvent, given the electrostatic repulsion that would exist between it and the reduced oxygen species.

Li_2O_2 electronic conductivity has been reported to increase with increasing temperature, via enhanced hole polaron transport, and therefore operating the battery at even slightly elevated temperatures should improve cell capacity.[42, 107] Higher temperature cell operation would therefore be another advantage, along with potentially improved stability, to employing molten salts or solid ion conductors as electrolytes. Doping of Li_2O_2 as it is electrochemically grown could also be a potential route to improving its conductivity.[123-125] To do so, an electrolyte additive (cations such as Co^{2+} and Ni^{2+}) would be added in minor quantities to the electrolyte. However, if doping were to succeed, reversible, concurrent deposition and oxidation of the dopant and Li_2O_2 would be necessarily required, which would be a challenging task.

3.3 Li_2O_2 conductivity's effect on charge

An intuitive assumption would be that once sufficient Li_2O_2 formation has resulted in sudden death during discharge, electronic resistance of the Li_2O_2 would necessarily result in a substantial overpotential during charge. However, in electrolytes where conformal Li_2O_2 coatings are observed (surface Li_2O_2 formation mechanism), Hojberg et al.[117] found that total cell impedance changed only slightly throughout the course of charge (always between 550-800 Ω at 220 μA/cm^2, Figure 9 c) and d)), with *iR* losses calculated from impedance only resulting in an expected overpotential of no more than ~200 mV, significantly lower than observed overpotentials at the end of charge in Figures 2a, 4a, 5a, and 9d. As a result, the ever-increasing charge overpotential

was instead ascribed by Hojberg et al. to a mixed potential related to the concomitant oxidation of Li_2O_2 to O_2 and Li_2O_2-induced electrolyte and carbon oxidation. These results were consistent with observations and calculations from Luntz et al.,[42] who postulated that application of an anodic (oxidative) overpotential would shift the Li_2O_2/positive electrode Fermi level closer to Li_2O_2's valence band maximum energy level. This energy gap reduction significantly reduces hole tunneling barriers and increases hole polaron concentration and conductivity during charge compared to discharge. In fact, cell impedance during charge was found by Hojberg et al. to be substantially lower than the estimated total cell impedance at sudden death during discharge (3 kΩ during a 220 $\mu A/cm^2$ rate).

In contrast to the small charge transport lengths needed through the conformal Li_2O_2 layers observed in a surface mechanism-dominant discharge, charge transport through large Li_2O_2 deposits is necessary to oxidize Li_2O_2 at the periphery of toroids when they are formed through the solution mechanism. Metallic-like electronic conductivity on the surface of stable Li_2O_2 facets has been calculated, although not experimentally verified.[126] However, impedance spectroscopy confirms that if Li_2O_2 surfaces are indeed metallic-like, they become electronically inaccessible to the conducting cathode matrix at the end of discharge.[117] It is therefore not clear how Li_2O_2 at the periphery of toroids is oxidized during charge, as it is then electronically isolated from the porous cathode by the bulk Li_2O_2 (given that transport lengths are prohibitive for tunneling and large for hole polarons), and it is insoluble in organic electrolytes, unlike LiO_2, so it cannot diffuse back to the cathode surface.

The use of soluble redox mediators and solubilizing agents. Although the oxidation mechanism of Li_2O_2 is not entirely understood when toroids are formed, a potential solution to the likely charge transport limitations is the inclusion of additives that are redox-active slightly above the potential of Li_2O_2 formation (e.g., 3.0-3.5V vs. Li/Li^+). Ideally, as the cell charges, the redox active molecule, termed a redox mediator, will oxidize at electronically accessible cathode sites and diffuse to the electronically isolated Li_2O_2, where a thermodynamically-favored outer sphere charge transfer can occur between the two molecules. By selecting a redox mediator with a redox potential slightly above the equilibrium potential of the Li-O_2 cell, O_2 evolution can theoretically occur at low observed overpotentials.

The idea of a redox mediator in the context of a Li-O_2 battery originated at Liox, where researchers explored a large variety of redox-active molecules to oxidize Li_2O_2, including substituted triarylamine, phenylenediamine, polyarylamine, phenothiazine, hydrazine, tetrathiafulvalene, thiophene, quinone, organometallic complexes, and various Li halides (e.g., LiI).[127] However, most redox mediators studied either exhibited poor stability or degraded the electrolyte solvent during operation; of course, improving the stability of the electrolyte may allow a redox mediator that exhibited the latter characteristic to function properly. Other reports have shown reasonable rechargeability using LiI[128] and tetrathiafulvalene,[129] although reports to the contrary have also been published.[7] Other possible redox mediators studied include a viologen derivative[130] and iron phthalocyanine.[131]

Of note, redox mediators have been used for overcharge protection in Li-ion batteries (redox mediators are typically termed redox shuttles in this context),[132-135] which raises an important consideration for the measurement of their Li_2O_2 oxidation efficacy. To impart overcharge protection in Li-ion batteries, the molecule's redox potential is selected to be slightly

higher (~0.3-0.4V) than the highest operating potential of the cell's positive electrode.[135] For example, 2,5-ditertbutyl-1,4-dimethoxybenzene, which has a reversible redox event at 3.9 V vs Li/Li^+, was used for overcharge protection in a $LiFePO_4$-based Li ion cell ($U_{LiFePO4}$~ 3.6 V vs Li/Li^+).[134] If overcharge occurs, which results in the potential of the positive electrode significantly increasing above its equilibrium potential, the redox mediator will in theory oxidize instead of the electrode material. It then diffuses to the negative electrode, where it is reduced, allowing it to diffuse back to the positive cathode to be oxidized again. Ideally, this shuttling mechanism is entirely reversible such that the overcharge could proceed indefinitely. A redox mediator in a Li-O_2 battery is intentionally selected to operate within the observed charge potential window, such that this indefinite shuttling behavior could proceed without necessarily oxidizing any Li_2O_2. This fact, combined with possible instability issues, requires the quantification of O_2 evolution Coulombic efficiency during charge when characterizing a newly developed redox mediator.

Another potential solution to the electron transport limitations imparted by Li_2O_2 toroid formation is to induce Li_2O_2 solubility to allow O_2^{2-} diffusion back to electronically accessible areas of the cathode during charge. To this end, anion receptors have been explored to enhance O_2^{2-} solubility, including strong Lewis acids such as tris(pentafluorophenyl) borane and boron esters.[136, 137] Unfortunately, these molecules tend to irreversibly degrade both chemically and electrochemically in Li-O_2 batteries, such that O_2 evolution from electrolytes containing them is very low.[138] This behavior likely results from the strong O_2^{2-} binding exhibited by the Lewis acid. Lowering the binding interaction between O_2^{2-} and the solubility-inducing additive may provide a route to a solution-soluble reversible O_2/O_2^{2-} couple. For example, cryptand cages have been reported to allow chemically reversible O_2 reduction to O_2^{2-}, although electrochemical reversibility of this or any other potential anion receptor would have to be verified using quantitative measures discussed in section 2.[139]

4. Conclusion

The allure of an ultra high-energy battery has prompted substantial research into the Li-O_2 electrochemical couple as a possible battery chemistry and significant progress has been made over the past decade in understanding the electrochemical processes occurring at the battery anode and cathode. However, expectations for a practical Li-air battery should be kept modest given the severity of the challenges facing the battery chemistry. Among necessary advances in other aspects of battery engineering, such as oxygen handling and purification, breakthroughs will be necessary to identify electrolytes and cathode materials stable to the Li-O_2 electrochemistry and to circumvent capacity limitations related to Li_2O_2 conductivity. We hope this Featured Article provides motivation for materials design that could provide solutions to these challenges.

5. Acknowledgements

The authors wish to thank Alan Luntz, Venkat Viswanathan, Dan Addison, and Wei Tong for helpful discussions. BDM, SER, and JEN gratefully acknowledge support through the Laboratory Directed Research and Development Program of Lawrence Berkeley National Laboratory under U.S. Department of Energy Contract No. DE-AC02-05CH11231, and support for CMB through the U.S. Department of Energy, Energy Efficiency and Renewable Energy Vehicle Technologies Office under award DE-0006869.

Table 1. A comparison of capacity, voltage and energy (disregarding weight of non-active battery components) of selected Li-based cathode materials for energy storage.

Active cathode material	Approximate reversible Li extraction/insertion[a] (x)	Theoretical specific capacity[b] (mAh/g)	Average discharge potential (V vs. Li/Li$^+$)	Typical voltage operating window (V vs. Li/Li$^+$)	Approximate theoretical specific energy (mWh/g)
$Li_{(1-x)}CoO_2$	0.6	164	3.8	4.2-3.7	625
$Li_{(1-x)}Mn_{1.5}Ni_{0.5}O_4$ (high-voltage spinel)	1	147	4.7	5.0-3.0	690
$Li_{(1-x)}Ni_{0.8}Co_{0.15}Al_{0.05}O_2$ (LiNCA)	0.7	195	3.8	4.2-2.0	740
$Li_{(1-x)}Ni_{0.33}Mn_{0.33}Co_{0.33}O_2$ (NMC333)	0.6	166	3.8	4.3-2.0	620
$Li_{(1.2-x)}Mn_{0.55}Ni_{0.15}Co_{0.10}O_2$ (LMR-NMC)	0.85	267	3.65	4.7-2.0	970
$Li_{(2-x)}O_2$	2	1168	2.85	4.5-2.0	3330
$Li_{(2-x)}S$	2	1168	2.15	2.5-1.5	2510

[a]Exact Li extraction, and therefore approximate specific energy, is a function of the upper operating voltage limit and rate of extraction employed

[b]calculated using the Li extraction provided in the second column

Values extracted/inferred from [1, 3, 9, 12, 14-16].

Table 2. e^-/O_2 during galvanostatic discharge and a comparison of oxygen evolution/consumption during a galvanostatic charge/discharge cycle for Li-O_2 cells employing various solvents. Values from [32].

Electrolyte solvent[a]	$(e^-/O_2)_{dis}$	OER/ORR
MPP-TFSI	2.30	0.33
DMSO	2.05	0.51
1NM3	2.14	0.48
NMP	1.96	0.58
THF	2.01	0.72
DME	2.01	0.78
CH_3CN	2.05	0.88
Triglyme	2.04	0.75

[a]MPP-TFSI: N-methyl-N-propylpiperidinium bis-(trifluoromethylsulfonyl) imide, DME : 1,2-dimethoxyethane, THF: tetrahydrofuran, TGE: triglyme, CH3CN: acetonitrile, DMSO: dimethyl sulfoxide, NMP: N-methyl pyrrolidone, 1NM3: tri(ethylene glycol)-substituted trimethylsilane.
Lithium tetrafluoroborate or lithium trifluoromethyl sulfonamide used as the electrolyte, carbon (XC72)-based cathode.

Table 3. Discharge Li_2O_2 yields for select Li-O_2 cells. Y_{Li2O2} is defined as the ratio of the amount of Li_2O_2 formed during a discharge to the amount of Li_2O_2 expected to form given a 2 e^- process. Values from [30].

Electrolyte	Cathode	Y_{Li2O2} (%)
1N LiTFSI/DME	P50	90.9±0.8
	PTFE-coated P50	90.3±1.1
	KB (PTFE-bound)	85.5±1.0
	Super P (PTFE-bound)	86.3±1.0
	XC72 (PTFE-bound)	83.3±0.5
	^{13}C (PTFE-bound)	77.2±0.7
	XC72 (Nafion-bound)	84.4±0.8
1N LiTFSI/1:1 EC:DMC	P50	9.8±1.2
1N LiTFSI/DMSO	P50	80.9±1.3
1N LiTriflate/Tetraglyme	P50	81.9±0.8

Table 4. Relative amounts of O_2 and CO_2 evolved from a cell employing carbon nanotubes decorated with Ru as cathodes and LiTriflate in DME as the electrolyte. Values from [94].

	Relative gas evolution	
Cycle #	**O_2**	**CO_2**
1	80	20
2	51	49
3	48	52
5	36	64
10	30	70
20	31	69
50	26	74

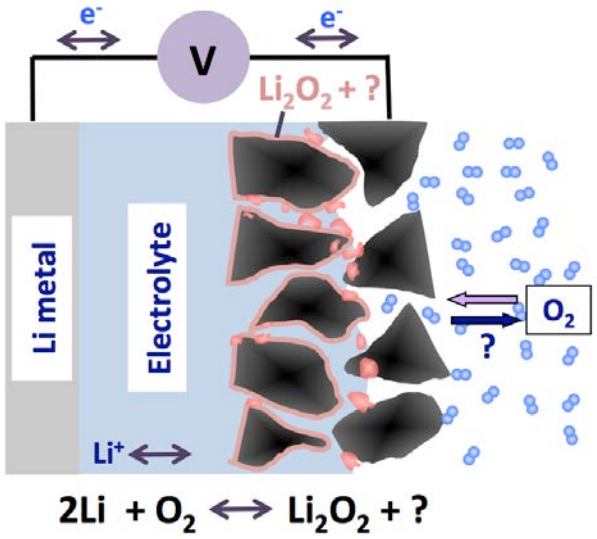

Figure 1. A schematic of a nonaqueous Li-O_2 battery. The dominant cathode chemistry is Li_2O_2 formation, although parasitic side products also form. Reprinted with permission from Ref. [7]. Copyright 2014 American Chemical Society.

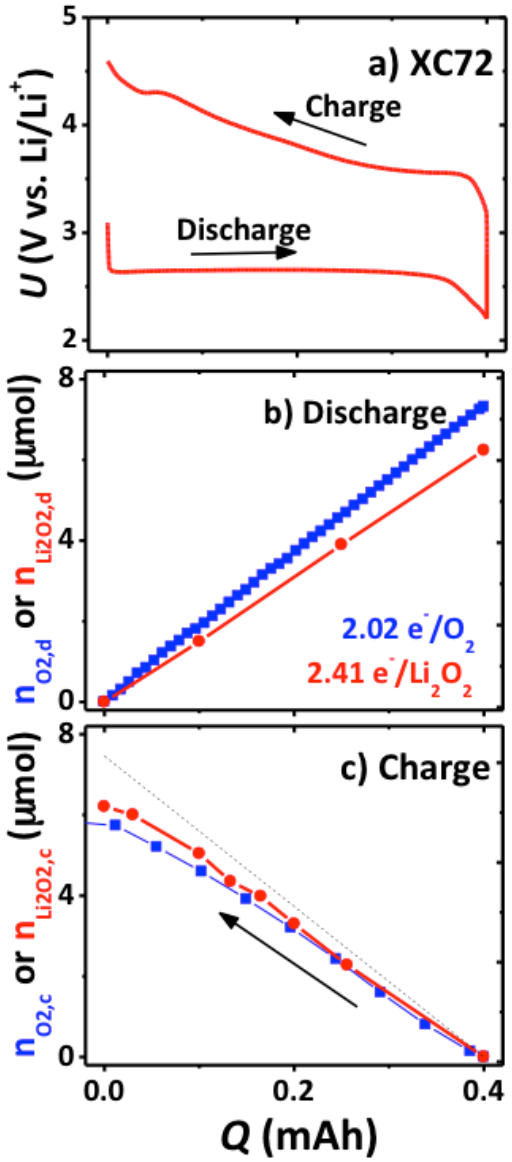

Figure 2. a) Galvanostatic discharge-charge of a Li-O_2 battery employing 1 N lithium trifluoromethyl sulfonimide (LiTFSI) in 1,2-dimethoxyethane (DME) as an electrolyte and XC72 bound to 316SS mesh using polytetrafluoroethylene (PTFE) as the cathode. **b)** quantitative O_2 consumption, $n_{O2,d}$, and Li_2O_2 formation, $n_{Li2O2,d}$, during discharge. **c)** Quantitative O_2 evolution, $n_{O2,c}$, and Li_2O_2 oxidation, $n_{Li2O2,c}$, during charge (the dashed black line indicates the ideal $2e^-$ process). Reprinted with permission from Ref. [30]. Copyright 2013 American Chemical Society.

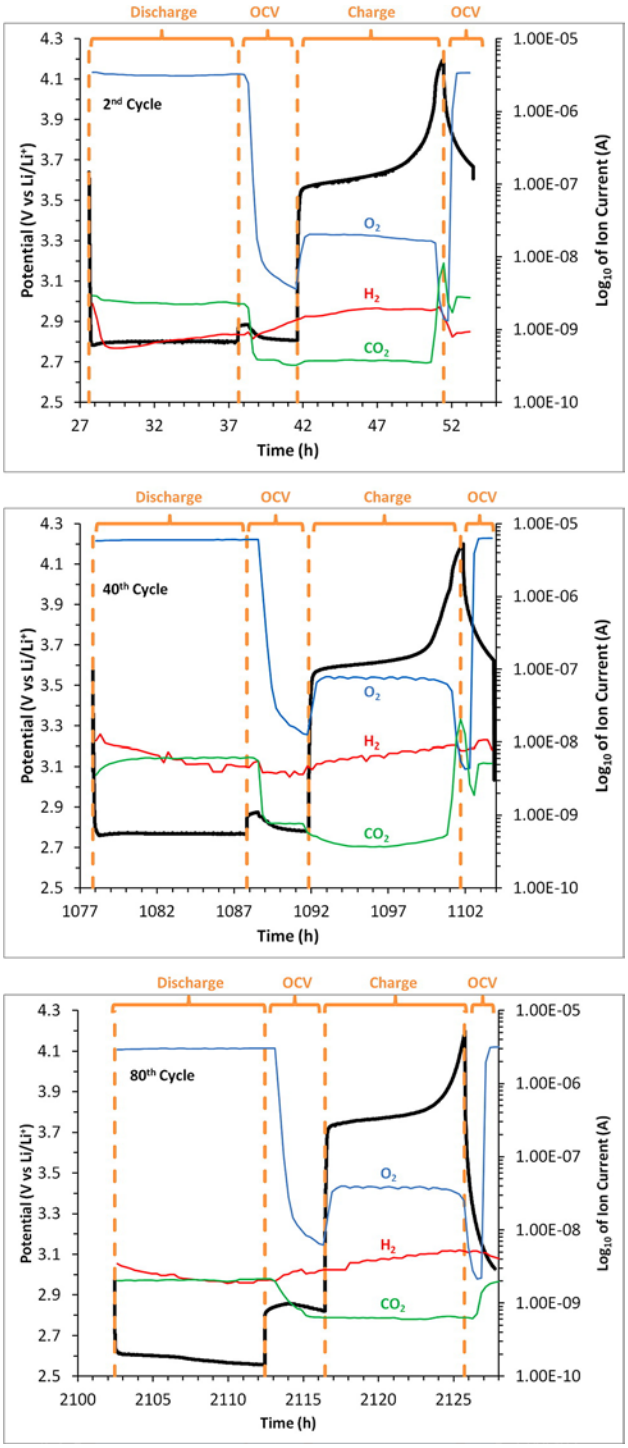

Figure 3. Gas evolution profile of the 2nd, 40th, and 80th cycle of a Li/1M $LiNO_3$ in dimethylacetamide/Super P carbon cell, room temperature, cycled at 0.1 mA/cm^2. Each cycle consisted of a discharge for 10 h under O_2, followed by a 4 h open circuit potential dwell to switch the gas environment from O_2 to Ar, followed by a charge to 4.2 V under Ar, and finally a 2 h OCV to switch from an Ar to O_2 environment. The higher baseline value for CO_2 during discharge is attributed to the increased oxidation of carbon impurities at the mass spectrometer filament under O_2. Reprinted with permission from Ref. [60]. Copyright 2013 American Chemical Society.

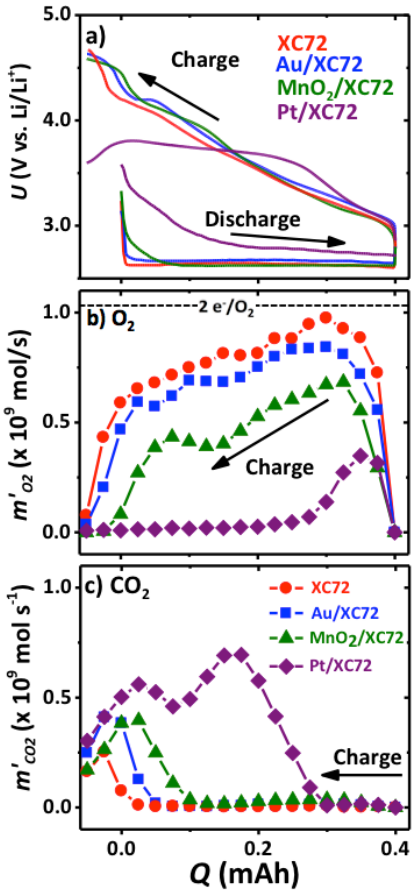

Figure 4. Gas evolution from cells employing DME. **a)** Discharge-charge voltage curves (0.2 mA total current), and corresponding O_2 **(b)** and CO_2 **(c)** evolution during charging of cells using various cathode catalysts. The Au, MnO_2, and Pt electrodes employed a 40wt% catalyst loading. Adapted with permission from Ref. [43]. Copyright 2011 American Chemical Society.

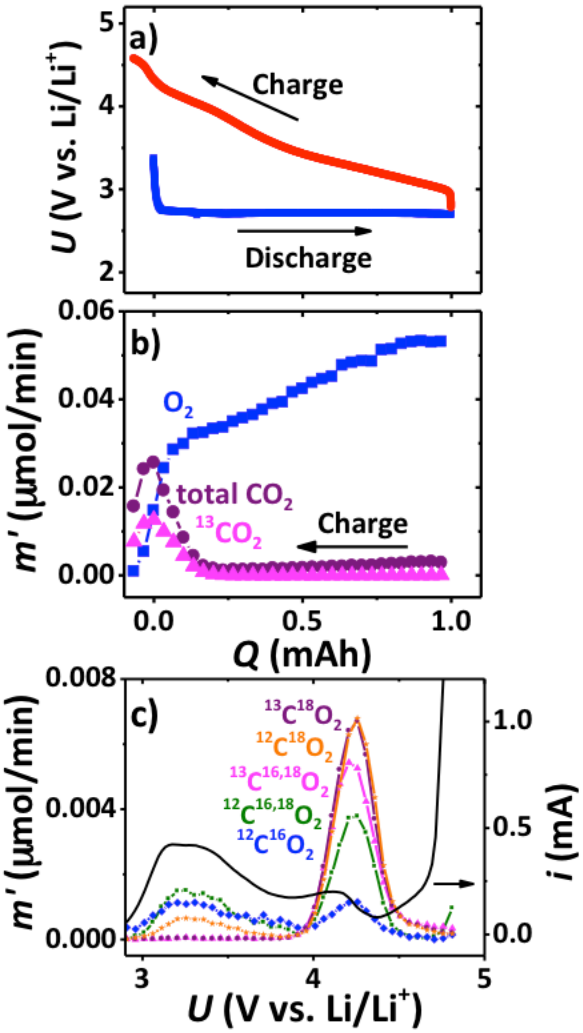

Figure 5. a) The first galvanostatic discharge-charge profile (0.2 mA total current) for a Li-O_2 cell employing a ^{13}C cathode and 1 M LiTFSI in DME. **b)** Quantitative evolution rates (m') for O_2, $^{13}CO_2$, and total CO_2 during the charge in a). An ideal 2 e^-/O_2 process would yield a constant O_2 evolution rate of 0.062 µmol/min. **c)** m' of various CO_2 isotopes during a linear sweep voltammogram (0.5 mV/s) following a galvanostatic discharge (1 mAh at 0.2 mA) of a cell employing a ^{13}C cathode, under an $^{18}O_2$ headspace. O_2 evolution not shown in c), but is roughly 50x larger than the total CO_2 evolution. Reprinted with permission from Ref. [44]. Copyright 2012 American Chemical Society.

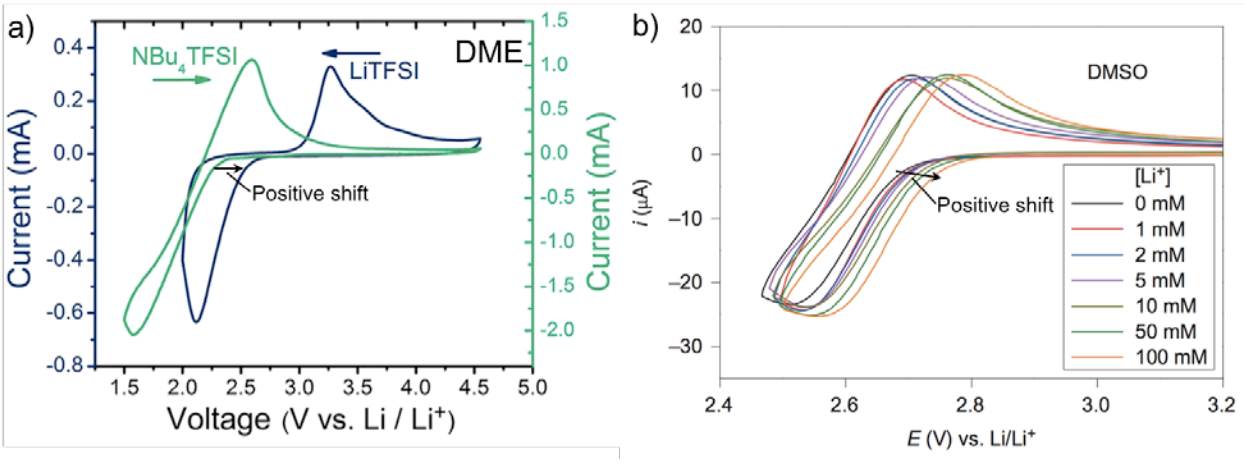

Figure 6. Cyclic voltammograms of O_2 reduction/evolution in 1M tetrabutyl ammonium or 1M LiTFSI in DME at a glassy carbon electrode **(a)** and varying ratios of NBu_4ClO_4:$LiClO_4$ (maintaining a total ClO_4^- concentration of 100 mM) in DMSO at a gold electrode **(b)**. In both cases, the onset of the cathodic scan is shifted positively when Li^+ is present (or $[Li^+]$ increases), implying that LiO_2 formation is the first step in the ORR in Li^+-bearing electrolytes, regardless of the electrolyte electron donor properties. **(a)** Adapted with permission from Ref. [113]. Copyright 2012 American Chemical Society. **(b)** Adapted with permission from Ref. [109]. Copyright 2014 Nature Publishing Group.

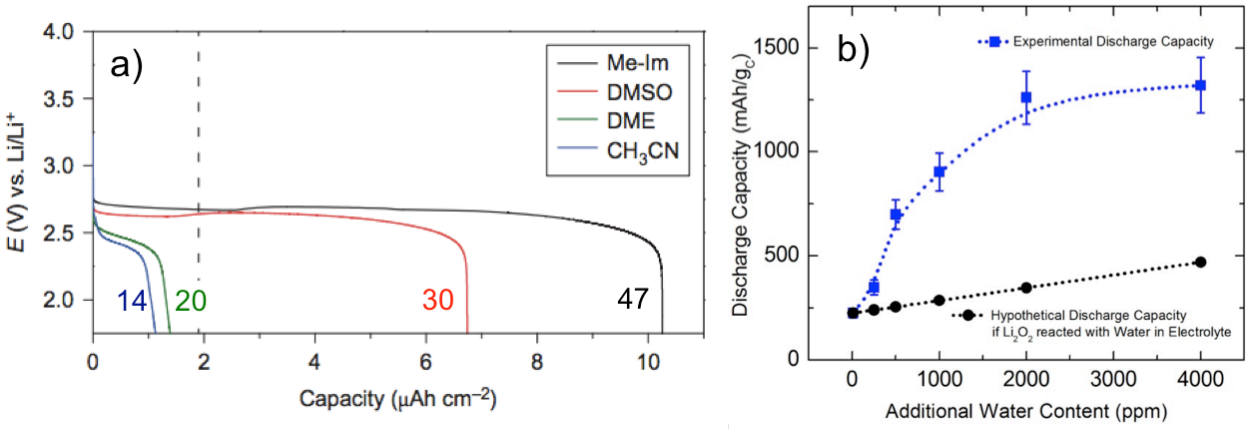

Figure 7. a) Potential versus time at a planar (nonporous) Au electrode in various O_2-saturated aprotic solvents and 100 mM $LiClO_4$. Me-Im: 1-methylimidazole. Numbers next to each discharge profile are the Gutmann donor numbers of the solvent employed in each cell. **b)** Experimental gravimetric discharge capacities (blue squares) for batteries with XC72 carbon cathodes and 1 M LiTFSI in DME with varying water content in the battery electrolyte (0.25 mA discharge to a cutoff voltage of 2.3 V). The black line in b) shows the hypothetical capacity gain from the chemical reaction of the water with Li_2O_2 to produce LiOH, which presumably dissolves from the surface of the cathode. This LiOH dissolution would free active sites and allow an equivalent amount of Li_2O_2 to be formed electrochemically. Comparing the observed capacity, the blue line, with this hypothetical limit it is clear that another mechanism besides LiOH formation accounts for the capacity gain. **(a)** Adapted with permission from Ref. [109]. Copyright 2014 Nature Publishing Group. **(b)** Reprinted with permission from Ref. [34]. Copyright 2015 Nature Publishing Group.

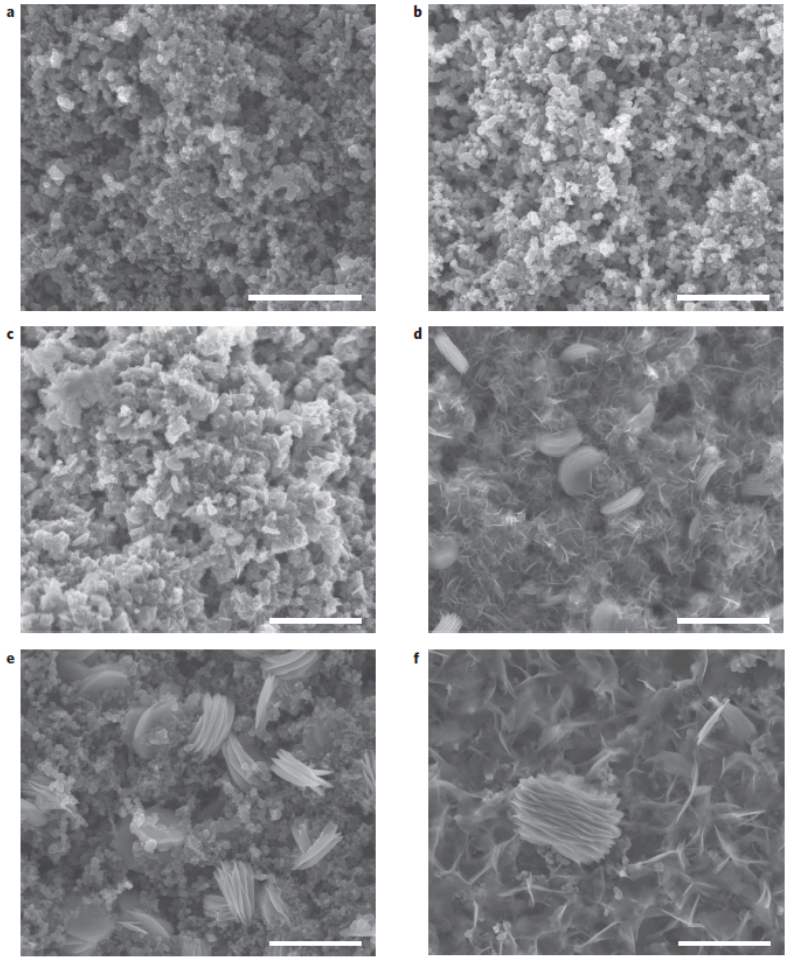

Figure 8. SEM images of a Vulcan XC72 carbon cathode without any discharge **(a)** and of similar cathodes discharged to a capacity of 1 mAh at a rate of 50 μA using nominally anhydrous (<30 ppm) 1M LiTFSI in DME as the electrolyte **(b)** and with water contents of 500 ppm **(c)**, 1000 ppm **(d)**, 2000 ppm **(e)**, and 4000 ppm **(f)** in the electrolyte. Cathodes were 12 mm in diameter and had a typical carbon loading of 1.5-2 mg. Scale bars are 1 μm. Reprinted with permission from Ref. [34]. Copyright 2015 Nature Publishing Group.

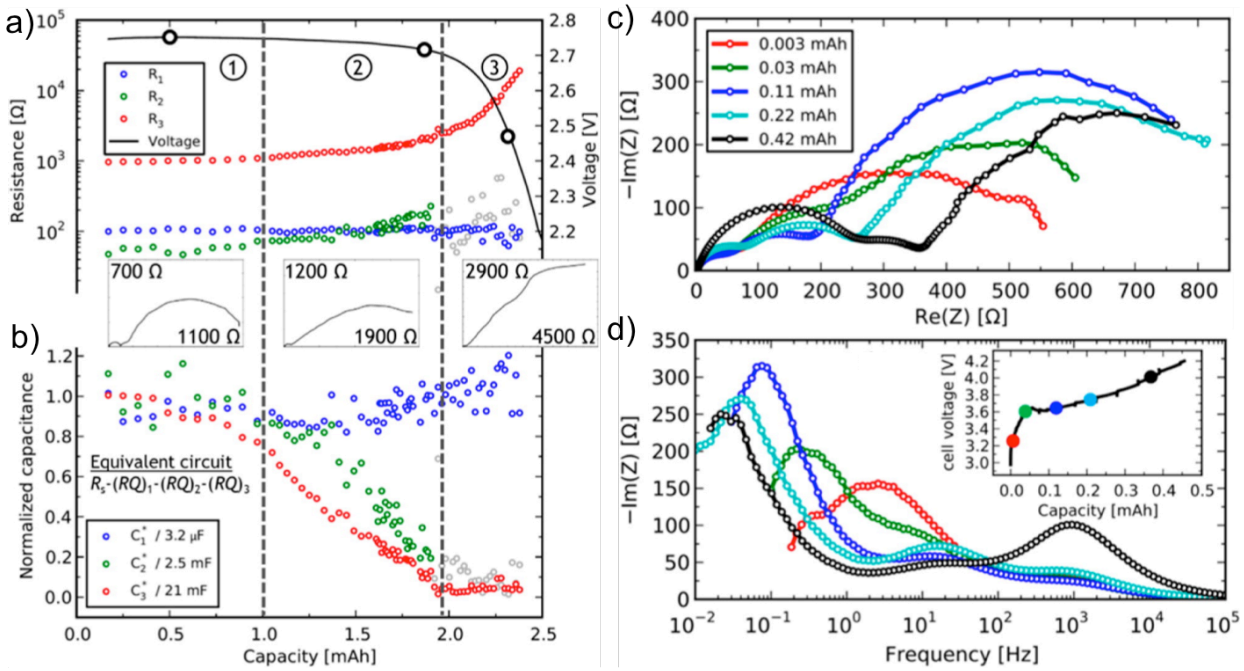

Figure 9. Resistances **(a)** and normalized pseudocapacitances **(b)** determined from electrochemical impedance spectroscopy measurements in a 18 μA/cm² constant current discharge to 2.2V. Nyquist plots are shown at three representative stages, and the corresponding states of discharge are marked with circles on the voltage profile. R_3 has been ascribed to oxygen reduction and electron transport through Li_2O_2. R_2 has been ascribed to another cathode process (perhaps binder degradation), and R_1 has been ascribed to a process occurring at the Li metal anode. Nyquist **(c)** and Bode-like **(d)** plots of EIS measurements made during a 220 μA/cm² constant current charge (traces color-coded to inset voltage profile) after a discharge to sudden death (2.0 V cutoff, total capacity of 0.46 mAh). Of note, the total impedance of the cell at sudden death during discharge was estimated to be 3 kΩ, significantly higher than all values measured during charge. Adapted with permission from Ref. [117]. Copyright 2015 American Chemical Society.

References

1. K. M. Abraham, *J. Phys. Chem. Lett.*, 2015, **6**, 830-844.
2. F. T. Wagner, B. Lakshmanan and M. F. Mathias, *J. Phys. Chem. Lett.*, 2010, **1**, 2204-2219.
3. M. S. Whittingham, *Chem. Rev.*, 2014, **114**, 11414-11443.
4. J. B. Goodenough and Y. Kim, *Chem. Mater.*, 2010, **22**, 587-603.
5. R. V. Noorden, *Nature*, 2014, **507**, 26-28.
6. M. N. Obrovac and V. L. Chevrier, *Chem. Rev.*, 2014, **114**, 11444-11502.
7. A. C. Luntz and B. D. McCloskey, *Chem. Rev.*, 2014, **114**, 11721-11750.
8. A. Manthiram, Y. Fu, S.-H. Chung, C. Zu and Y.-S. Su, *Chem. Rev.*, 2014, **114**, 11751-11787.
9. X. Ji and L. F. Nazar, *J. Mater. Chem.*, 2010, **20**, 9821-9826.
10. I. Shterenberg, M. Salama, Y. Gofer, E. Levi and D. Aurbach, *MRS Bulletin*, 2014, **39**, 453-460.
11. J. Muldoon, C. B. Bucur and T. Gregory, *Chem. Rev.*, 2014, **114**, 11683-11720.
12. J. W. Fergus, *J. Power Sources*, 2010, **195**, 939-954.
13. Z. Li, N. A. Chernova, J. Feng, S. Upreti, F. Omenya and M. S. Whittingham, *J. Electrochem. Soc.*, 2011, **159**, A116-A120.

14. M. Bettge, Y. Li, K. Gallagher, Y. Zhu, Q. Wu, W. Lu, I. Bloom and D. P. Abraham, *J. Electrochem. Soc.*, 2013, **160**, A2046-A2055.
15. T. Ohzuku, S. Takeda and M. Iwanaga, *J. Power Sources*, 1999, **81–82**, 90-94.
16. F. Lin, I. M. Markus, D. Nordlund, T.-C. Weng, M. D. Asta, H. L. Xin and M. M. Doeff, *Nature Comm.*, 2014, **5**.
17. G. Girishkumar, B. McCloskey, A. C. Luntz, S. Swanson and W. Wilcke, *J. Phys. Chem. Lett.*, 2010, **1**, 2193-2203.
18. P. G. Bruce, S. A. Freunberger, L. J. Hardwick and J.-M. Tarascon, *Nature Mater.*, 2012, **11**, 19-29.
19. J. Christensen, P. Albertus, R. S. Sanchez-Carrera, T. Lohmann, B. Kozinsky, R. Liedtke, J. Ahmed and A. Kojic, *J. Electrochem. Soc.*, 2012, **159**, R1-R30.
20. J. Lu, L. Li, J.-B. Park, Y.-K. Sun, F. Wu and K. Amine, *Chem. Rev.*, 2014, **114**, 5611-5640.
21. K. G. Gallagher, S. Goebel, T. Greszler, M. Mathias, W. Oelerich, D. Eroglu and V. Srinivasan, *Energy Environ. Sci.*, 2014, **7**, 1555-1563.
22. D. G. Kwabi, N. Ortiz-Vitoriano, S. A. Freunberger, Y. Chen, N. Imanishi, P. G. Bruce and Y. Shao-Horn, *MRS Bulletin*, 2014, **39**, 443-452.
23. A. Kraytsberg and Y. Ein-Eli, *J. Power Sources*, 2011, **196**, 886-893.
24. L. Li, X. Zhao and A. Manthiram, *Electrochem. Commun.*, 2012, **14**, 78-81.
25. S. J. Visco and Y. S. Nimon, US Patent #7,645,543, 2010.
26. T. Zhang, N. Imanishi, Y. Shimonishi, A. Hirano, Y. Takeda, O. Yamamoto and N. Sammes, *Chem. Commun.*, 2010, **46**, 1661-1663.
27. Y. Wang and H. Zhou, *J. Power Sources*, 2010, **195**, 358-361.
28. S. J. Visco, L. C. De Jonghe, Y. S. Nimon, A. Petrov and K. Pridatko, US Patent #8,323,820, 2012.
29. A. Galbraith, *The lithium-water-air battery for automotive propulsion, Union Internationale des Producteurs et Distributeurs d'Energie Electrique and Electric Vehicle Council, 4th International Electric Vehicle Symposium*, 1976, **1**.
30. B. D. McCloskey, A. Valery, A. C. Luntz, S. R. Gowda, G. M. Wallraff, J. M. Garcia, T. Mori and L. E. Krupp, *J. Phys. Chem. Lett.*, 2013, **4**, 2989- 2993.
31. K. M. Abraham and Z. Jiang, *J. Electrochem. Soc.*, 1996, **143**, 1-5.
32. B. D. McCloskey, D. S. Bethune, R. M. Shelby, T. Mori, R. Scheffler, A. Speidel, M. Sherwood and A. C. Luntz, *J. Phys. Chem. Lett.*, 2012, **3**, 3043-3047.
33. W. Xu, J. Hu, M. H. Engelhard, S. A. Towne, J. S. Hardy, J. Xiao, J. Feng, M. Y. Hu, J. Zhang, F. Ding, M. E. Gross and J.-G. Zhang, *J. Power Sources*, 2012, **215**, 240-247.
34. N. B. Aetukuri, B. D. McCloskey, J. M. García, L. E. Krupp, V. Viswanathan and A. C. Luntz, *Nature Chem.*, 2015, **7**, 50-56.
35. K. U. Schwenke, M. Metzger, T. Restle, M. Piana and H. A. Gasteiger, *J. Electrochem. Soc.*, 2015, **162**, A573-A584.
36. M. Leskes, A. J. Moore, G. R. Goward and C. P. Grey, *J. Phys. Chem. C*, 2013, **117**, 26929-26939.
37. M. Leskes, N. E. Drewett, L. J. Hardwick, P. G. Bruce, G. R. Goward and C. P. Grey, *Angew. Chem.*, 2012, **124**, 8688-8691.
38. Z. Peng, S. A. Freunberger, L. J. Hardwick, Y. Chen, V. Giordani, F. Barde, P. Novak, D. Graham, J.-M. Tarascon and P. G. Bruce, *Angew. Chem., Int. Ed.*, 2011, **50**, 6351-6355.
39. J. Yang, D. Zhai, H.-H. Wang, K. C. Lau, J. A. Schlueter, P. Du, D. J. Myers, Y.-K. Sun, L. A. Curtiss and K. Amine, *Phys. Chem. Chem. Phys.*, 2013, **15**, 3764-3771.
40. D. Zhai, K. C. Lau, H.-H. Wang, J. Wen, D. J. Miller, J. Lu, F. Kang, B. Li, W. Yang, J. Gao, E. Indacochea, L. A. Curtiss and K. Amine, *Nano Lett.*, 2015, **15**, 1041-1046.
41. V. Viswanathan, K. S. Thygesen, J. S. Hummelshoj, J. K. Norskov, G. Girishkumar, B. D. McCloskey and A. C. Luntz, *J. Chem. Phys.*, 2011, **135**, 214704.

42. A. C. Luntz, V. Viswanathan, J. Voss, J. B. Varley, J. K. Nørskov, R. Scheffler and A. Speidel, *J. Phys. Chem. Lett.*, 2013, **4**, 3494- 3499.
43. B. D. McCloskey, R. Scheffler, A. Speidel, D. S. Bethune, R. M. Shelby and A. C. Luntz, *J. Am. Chem. Soc.*, 2011, **133**, 18038-18041.
44. B. D. McCloskey, A. Speidel, R. Scheffler, D. C. Miller, V. Viswanathan, J. S. Hummelshøj, J. K. Nørskov and A. C. Luntz, *J. Phys. Chem. Lett.*, 2012, **3**, 997-1001.
45. B. D. McCloskey, D. S. Bethune, R. M. Shelby, G. Girishkumar and A. C. Luntz, *J. Phys. Chem. Lett.*, 2011, **2**, 1161-1166.
46. C. J. Barile and A. A. Gewirth, *J. Electrochem. Soc.*, 2013, **160**, A549-A552.
47. N. Tsiouvaras, S. Meini, I. Buchberger and H. A. Gasteiger, *J. Electrochem. Soc.*, 2013, **160**, A471-A477.
48. F. Mizuno, S. Nakanishi, Y. Kotani, S. Yokoishi and H. Iba, *Electrochemistry*, 2010, **78**, 403-405.
49. S. A. Freunberger, Y. Chen, Z. Peng, J. M. Griffin, L. J. Hardwick, F. Barde, P. Novak and P. G. Bruce, *J. Am. Chem. Soc.*, 2011, **133**, 8040-8047.
50. V. S. Bryantsev and M. Blanco, *J. Phys. Chem. Lett.*, 2011, **2**, 379-383.
51. W. Xu, K. Xu, V. V. Viswanathan, S. A. Towne, J. S. Hardy, J. Xiao, D. Hu, D. Wang and J.-G. Zhang, *J. Power Sources*, 2011, **196**, 9631-9639.
52. G. M. Veith, J. Nanda, L. H. Delmau and N. J. Dudney, *J. Phys. Chem. Lett.*, 2012, **3**, 1242-1247.
53. E. Nasybulin, W. Xu, M. H. Engelhard, Z. Nie, S. D. Burton, L. Cosimbescu, M. E. Gross and J.-G. Zhang, *J. Phys. Chem. C*, 2013, **117**, 2635-2645.
54. J. Xiao, J. Hu, D. Wang, D. Hu, W. Xu, G. L. Graff, Z. Nie, J. Liu and J.-G. Zhang, *J. Power Sources*, 2011, **196**, 5674-5678.
55. R. Younesi, M. Hahlin and K. Edström, *ACS Appl. Mater. Interfaces*, 2013, **5**, 1333-1341.
56. V. S. Bryantsev, J. Uddin, V. Giordani, W. Walker, D. Addison and G. V. Chase, *J. Electrochem. Soc.*, 2013, **160**, A160-A171.
57. V. S. Bryantsev and F. Faglioni, *J. Phys. Chem. A*, 2012, **116**, 7128-7138.
58. V. S. Bryantsev, V. Giordani, W. Walker, M. Blanco, S. Zecevic, K. Sasaki, J. Uddin, D. Addison and G. V. Chase, *J. Phys. Chem. A*, 2011, **115**, 12399-12409.
59. V. Giordani, V. S. Bryantsev, J. Uddin, W. Walker, G. V. Chase and D. Addison, *ECS Electrochem. Lett.*, 2014, **3**, A11-A14.
60. W. Walker, V. Giordani, J. Uddin, V. S. Bryantsev, G. V. Chase and D. Addison, *J. Am. Chem. Soc.*, 2013, **135**, 2076-2079.
61. S. A. Freunberger, Y. Chen, N. E. Drewett, L. J. Hardwick, F. Bardé and P. G. Bruce, *Angew. Chem., Int. Ed.*, 2011, **50**, 8609-8613.
62. Y. Chen, S. A. Freunberger, Z. Peng, F. Bardé and P. G. Bruce, *J. Am. Chem. Soc.*, 2012, **134**, 7952-7957.
63. F. Bardé, Y. Chen, L. Johnson, S. Schaltin, J. Fransaer and P. G. Bruce, *J. Phys. Chem. C*, 2014, **118**, 18892-18898.
64. Z. Peng, S. A. Freunberger, Y. Chen and P. G. Bruce, *Science*, 2012, **337**, 563-566.
65. D. Sharon, M. Afri, M. Noked, A. Garsuch, A. A. Frimer and D. Aurbach, *J. Phys. Chem. Lett.*, 2013, **4**, 3115-3119.
66. R. Younesi, P. Norby and T. Vegge, *ECS Electrochem. Lett.*, 2014, **3**, A15-A18.
67. D. G. Kwabi, T. P. Batcho, C. V. Amanchukwu, N. Ortiz-Vitoriano, P. Hammond, C. V. Thompson and Y. Shao-Horn, *J. Phys. Chem. Lett.*, 2014, **5**, 2850-2856.
68. N. Mozhzhukhina, L. P. Méndez De Leo and E. J. Calvo, *J. Phys. Chem. C*, 2013, **117**, 18375-18380.
69. V. S. Bryantsev, *Chem. Phys. Lett.*, 2013, **558**, 42-47.
70. A. Khetan, A. Luntz and V. Viswanathan, *J. Phys. Chem. Lett.*, 2015, 1254-1259.

71. R. S. Assary, K. C. Lau, K. Amine, Y.-K. Sun and L. A. Curtiss, *J. Phys. Chem. C*, 2013, **117**, 8041-8049.
72. J. M. García, H. W. Horn and J. E. Rice, *J. Phys. Chem. Lett.*, 2015, **6**, 1795-1799.
73. R. Murugan, V. Thangadurai and W. Weppner, *Angew. Chem. Int. Ed.*, 2007, **46**, 7778-7781.
74. F. Li, H. Kitaura and H. Zhou, *Energy Environ. Sci.*, 2013, **6**, 2302-2311.
75. B. Kumar, J. Kumar, R. Leese, J. P. Fellner, S. J. Rodrigues and K. M. Abraham, *J. Electrochem. Soc.*, 2010, **157**, A50-A54.
76. L. Cheng, W. Chen, M. Kunz, K. Persson, N. Tamura, G. Chen and M. Doeff, *ACS Appl. Mater. Interfaces*, 2015, **7**, 2073-2081.
77. M. Kotobuki, H. Munakata, K. Kanamura, Y. Sato and T. Yoshida, *J. Electrochem. Soc.*, 2010, **157**, A1076-A1079.
78. N. Kamaya, K. Homma, Y. Yamakawa, M. Hirayama, R. Kanno, M. Yonemura, T. Kamiyama, Y. Kato, S. Hama, K. Kawamoto and A. Mitsui, *Nature Mater.*, 2011, **10**, 682-686.
79. S. P. Ong, Y. Mo, W. D. Richards, L. Miara, H. S. Lee and G. Ceder, *Energy Environ. Sci.*, 2013, **6**, 148-156.
80. P. Hartmann, T. Leichtweiss, M. R. Busche, M. Schneider, M. Reich, J. Sann, P. Adelhelm and J. Janek, *J. Phys. Chem. C*, 2013, **117**, 21064-21074.
81. J. Uddin, D. D. Addison, V. Giordani, G. V. Chase and W. Walker, Patent #WO 2014153551, 2014.
82. A. Lewandowski and A. Świderska-Mocek, *J. Power Sources*, 2009, **194**, 601-609.
83. T. Kuboki, T. Okuyama, T. Ohsaki and N. Takami, *J. Power Sources*, 2005, **146**, 766-769.
84. C. J. Allen, S. Mukerjee, E. J. Plichta, M. A. Hendrickson and K. M. Abraham, *J. Phys. Chem. Lett.*, 2011, **2**, 2420-2424.
85. J. Hassoun, F. Croce, M. Armand and B. Scrosati, *Angew. Chem. Int. Ed.*, 2011, **50**, 2999-3002.
86. A. Khetan, H. Pitsch and V. Viswanathan, *J. Phys. Chem. Lett.*, 2014, **5**, 1318-1323.
87. A. Khetan, H. Pitsch and V. Viswanathan, *J. Phys. Chem. Lett.*, 2014, **5**, 2419-2424.
88. Y.-C. Lu, H. A. Gasteiger and Y. Shao-Horn, *J. Am. Chem. Soc.*, 2011, **133**, 19048-19051.
89. Y. Shao, S. Park, J. Xiao, J.-G. Zhang, Y. Wang and J. Liu, *ACS Catalysis*, 2012, **2**, 844-857.
90. V. Viswanathan, J. K. Nørskov, A. Speidel, R. Scheffler, S. Gowda and A. C. Luntz, *J. Phys. Chem. Lett.*, 2013, **4**, 556-560.
91. J. S. Hummelshoj, A. C. Luntz and J. K. Norskov, *J. Chem. Phys.*, 2013, **138**, 034703.
92. M. M. Ottakam Thotiyl, S. A. Freunberger, Z. Peng and P. G. Bruce, *J. Am. Chem. Soc.*, 2013, **135**, 494-500.
93. S. R. Gowda, A. Brunet, G. M. Wallraff and B. D. McCloskey, *J. Phys. Chem. Lett.*, 2013, **4**, 276-279.
94. E. N. Nasybulin, W. Xu, B. L. Mehdi, E. Thomsen, M. H. Engelhard, R. C. Massé, P. Bhattacharya, M. Gu, W. Bennett, Z. Nie, C. Wang, N. D. Browning and J.-G. Zhang, *ACS Appl. Mater. Interfaces*, 2014, **6**, 14141-14151.
95. B. M. Gallant, R. R. Mitchell, D. G. Kwabi, J. Zhou, L. Zuin, C. V. Thompson and Y. Shao-Horn, *J. Phys. Chem. C*, 2012, **116**, 20800-20805.
96. D. M. Itkis, D. A. Semenenko, E. Y. Kataev, A. I. Belova, V. S. Neudachina, A. P. Sirotina, M. Hävecker, D. Teschner, A. Knop-Gericke, P. Dudin, A. Barinov, E. A. Goodilin, Y. Shao-Horn and L. V. Yashina, *Nano Lett.*, 2013, **13**, 4697-4701.
97. R. Black, S. H. Oh, J.-H. Lee, T. Yim, B. Adams and L. F. Nazar, *J. Am. Chem. Soc.*, 2012, **134**, 2902-2905.
98. E. Nasybulin, W. Xu, M. H. Engelhard, Z. Nie, X. S. Li and J.-G. Zhang, *J. Power Sources*, 2013, **243**, 899-907.
99. C. V. Amanchukwu, J. R. Harding, Y. Shao-Horn and P. T. Hammond, *Chem. Mater.*, 2015, **27**, 550-561.

100. M. M. Ottakam Thotiyl, S. A. Freunberger, Z. Peng, Y. Chen, Z. Liu and P. G. Bruce, *Nature Mater.*, 2013, **12**, 1050-1056.
101. B. D. Adams, R. Black, C. Radtke, Z. Williams, B. L. Mehdi, N. D. Browning and L. F. Nazar, *ACS Nano*, 2014, **8**, 12483-12493.
102. A. Riaz, K.-N. Jung, W. Chang, K.-H. Shin and J.-W. Lee, *ACS Appl. Mater. Interfaces*, 2014, **6**, 17815-17822.
103. H. Lee, Y.-J. Kim, D. J. Lee, J. Song, Y. M. Lee, H.-T. Kim and J.-K. Park, *J. Mater. Chem. A*, 2014, **2**, 11891-11898.
104. Y. Cui, Z. Wen and Y. Liu, *Energy Environ. Sci.*, 2011, **4**, 4727-4734.
105. J. Lu, Y. Lei, K. C. Lau, X. Luo, P. Du, J. Wen, R. S. Assary, U. Das, D. J. Miller, J. W. Elam, H. M. Albishri, D. Abd El-Hady, Y.-K. Sun, L. A. Curtiss and K. Amine, *Nature Comm.*, 2013, **4**, 2383.
106. J. Xie, X. Yao, Q. Cheng, I. P. Madden, P. Dornath, C.-C. Chang, W. Fan and D. Wang, *Angew. Chem.*, 2015, **127**, 4373-4377.
107. O. Gerbig, R. Merkle and J. Maier, *Adv. Mat.*, 2013, **25**, 3129-3133.
108. J. B. Varley, V. Viswanathan, J. K. Norskov and A. C. Luntz, *Energy Environ. Sci.*, 2014, **7**, 720-727.
109. L. Johnson, C. Li, Z. Liu, Y. Chen, S. A. Freunberger, P. C. Ashok, B. B. Praveen, K. Dholakia, J.-M. Tarascon and P. G. Bruce, *Nature Chem.*, 2014, **6**, 1091-1099.
110. C. O. Laoire, S. Mukerjee, K. M. Abraham, E. J. Plichta and M. A. Hendrickson, *J. Phys. Chem. C*, 2010, **114**, 9178-9186.
111. C. O. Laoire, S. Mukerjee, K. M. Abraham, E. J. Plichta and M. A. Hendrickson, *J. Phys. Chem. C*, 2009, **113**, 20127-20134.
112. W. Torres, N. Mozhzhukhina, A. Y. Tesio and E. J. Calvo, *J. Electrochem. Soc.*, 2014, **161**, A2204-A2209.
113. B. D. McCloskey, R. Scheffler, A. Speidel, G. Girishkumar and A. C. Luntz, *J. Phys. Chem. C*, 2012, **116**, 23897-23905.
114. R. Cao, E. D. Walter, W. Xu, E. N. Nasybulin, P. Bhattacharya, M. E. Bowden, M. H. Engelhard and J.-G. Zhang, *ChemSusChem*, 2014, **7**, 2436-2440.
115. I. L. Vol'nov, S. A. Tokareva, V. N. Belevskii and V. I. Klimanov, *Izvestiya Akademii Nauk SSRR, Ser. Khim.*, 1967, **7**, 1411-1414.
116. S. Meini, M. Piana, N. Tsiouvaras, A. Garsuch and H. A. Gasteiger, *Electrochem. Solid-State Lett.*, 2012, **15**, A45-A48.
117. J. Højberg, B. D. McCloskey, J. Hjelm, T. Vegge, K. Johansen, P. Norby and A. C. Luntz, *ACS Appl. Mater. Interfaces*, 2015, **7**, 4039-4047.
118. S. Meini, M. Piana, H. Beyer, J. Schwämmlein and H. A. Gasteiger, *J. Electrochem. Soc.*, 2012, **159**, A2135-A2142.
119. B. D. Adams, C. Radtke, R. Black, M. L. Trudeau, K. Zaghib and L. F. Nazar, *Energy Environ. Sci.*, 2013, **6**, 1772-1778.
120. Y. C. Lu, B. M. Gallant, D. G. Kwabi, J. R. Harding, R. R. Mitchell, M. S. Whittingham and Y. Shao-Horn, *Energy Environ. Sci.*, 2013, **6**, 750-768.
121. I. Gunasekara, S. Mukerjee, E. J. Plichta, M. A. Hendrickson and K. M. Abraham, *J. Electrochem. Soc.*, 2015, **162**, A1055-A1066.
122. C. M. Burke, V. Pande, A. Khetan, V. Viswanathan and B. D. McCloskey, *arXiv preprint arXiv:1503.07925*, 2015.
123. V. Timoshevskii, Z. Feng, K. H. Bevan, J. Goodenough and K. Zaghib, *Appl. Phys. Lett.*, 2013, **103**, 073901.
124. Y. Zhao, C. Ban, J. Kang, S. Santhanagopalan, G.-H. Kim, S.-H. Wei and A. C. Dillon, *Appl. Phys. Lett.*, 2012, **101**.
125. M. D. Radin, C. W. Monroe and D. J. Siegel, *Chem. Mater.*, 2015, **27**, 839-847.
126. M. D. Radin, J. F. Rodriguez, F. Tian and D. J. Siegel, *J. Am. Chem. Soc.*, 2012, **134**, 1093-1103.

127. G. V. Chase, S. Zecevic, W. Walker, J. Uddin, K. A. Sasaki, V. Giordani, V. Bryantsev, M. Blanco and D. D. Addison, US patent app. #13/093,759, 2011.
128. H.-D. Lim, H. Song, J. Kim, H. Gwon, Y. Bae, K.-Y. Park, J. Hong, H. Kim, T. Kim, Y. H. Kim, X. Lepró, R. Ovalle-Robles, R. H. Baughman and K. Kang, *Angew. Chem. Int. Ed.*, 2014, **53**, 3926-3931.
129. Y. Chen, S. A. Freunberger, Z. Peng, O. Fontaine and P. G. Bruce, *Nature Chem.*, 2013, **5**, 489-494.
130. M. J. Lacey, J. T. Frith and J. R. Owen, *Electrochem. Commun.*, 2013, **26**, 74-76.
131. D. Sun, Y. Shen, W. Zhang, L. Yu, Z. Yi, W. Yin, D. Wang, Y. Huang, J. Wang, D. Wang and J. B. Goodenough, *J. Am. Chem. Soc.*, 2014, **136**, 8941-8946.
132. K. M. Abraham and D. M. Pasquariello, US patent #4,857,423, 1989.
133. T. J. Richardson and P. N. Ross, *J. Electrochem. Soc.*, 1996, **143**, 3992-3996.
134. J. R. Dahn, J. Jiang, L. M. Moshurchak, M. D. Fleischauer, C. Buhrmester and L. J. Krause, *J. Electrochem. Soc.*, 2005, **152**, A1283-A1289.
135. J. Chen, C. Buhrmester and J. R. Dahn, *Electrochem. Solid-State Lett.*, 2005, **8**, A59-A62.
136. B. Xie, H. S. Lee, H. Li, X. Q. Yang, J. McBreen and L. Q. Chen, *Electrochem. Commun.*, 2008, **10**, 1195-1197.
137. D. Shanmukaraj, S. Grugeon, G. Gachot, S. Laruelle, D. Mathiron, J.-M. Tarascon and M. Armand, *J. Am. Chem. Soc.*, 2010, **132**, 3055-3062.
138. A. C. Luntz, B. D. McCloskey, S. Gowda, H. Horn and V. Viswanathan, in *The Lithium Air Battery*, eds. N. Imanishi, A. C. Luntz and P. Bruce, Springer New York, 2014, ch. 3, pp. 59-120.
139. N. Lopez, D. J. Graham, R. McGuire, G. E. Alliger, Y. Shao-Horn, C. C. Cummins and D. G. Nocera, *Science*, 2012, **335**, 450-453.